EGG-TMI-8133.

Idaho
National
Engineering
Laboratory

Managed
by the U.S.
Department
of Energy

EGG-TMI-8133
August 1988

PATENT CLEARED

INFORMAL REPORT

TMI-2 LOWER HEAD CREEP RUPTURE ANALYSIS

G. L. Thinnes

LOAN COPY
THIS REPORT MAY BE RECALLED
AFTER TWO WEEKS PLEASE
RETURN PROMPTLY TO:
TECHNICAL LIBRARY

Steven Chavez 11-27-90
M C Russell 1/18/91

EG&G Idaho

Work performed under
DOE Contract
No. DE-AC07-76ID01570

DISCLAIMER

This book was prepared as an account of work sponsored by an agency of the United States Government. Neither the United States Government nor any agency thereof, nor any of their employees, makes any warranty, express or implied, or assumes any legal liability or responsibility for the accuracy, completeness, or usefulness of any information, apparatus, product or process disclosed, or represents that its use would not infringe privately owned rights. References herein to any specific commercial product, process, or service by trade name, trademark, manufacturer, or otherwise, does not necessarily constitute or imply its endorsement, recommendation, or favoring by the United States Government or any agency thereof. The views and opinions of authors expressed herein do not necessarily state or reflect those of the United States Government or any agency thereof.

EGG-TMI-8133

TMI-2 LOWER HEAD CREEP RUPTURE ANALYSIS

Gary L. Thinnes

Published August 1988

EG&G Idaho, Inc.
Idaho Falls, Idaho 83415

Prepared for the
U.S. Department of Energy
Idaho Operations Office
Under DOE Contract No. DE-AC07-76ID01570

ABSTRACT

The TMI-2 accident resulted in approximately 40% of the reactor's core melting and collecting on the lower head of the reactor pressure vessel. The severity of the accident has raised questions about the margin of safety against rupture of the lower head in this accident since all evidence seems to indicate no major breach of the vessel occurred. Scoping heat transfer analyses of the relocated core debris and lower head have been made based upon assumed core melting scenarios and core material debris formations while in contact with the lower head.

This report describes the structural finite element creep rupture analysis of the lower head using a temperature transient judged most likely to challenge the structural capacity of the vessel. This evaluation of vessel response to this transient has provided insight into the creep mechanisms of the vessel wall, a realistic mode of failure, and a means by which margin to failure can be evaluated once examination provides estimated maximum wall temperatures. Suggestions for more extensive research in this area are also provided.

SUMMARY

The lower head of the TMI-2 reactor pressure vessel (RPV) withstood a considerable thermal challenge from the 15 to 20 metric tons of molten core material which settled upon it during the TMI-2 accident. Interpretation of the TMI-2 instrumentation measurements suggests that the molten core material settled from the core to the lower head in less than one minute. Important questions remain to be answered regarding the heat transfer from the core debris to the head, the localized damage to the head, and margin-to-failure of the lower head. These questions are of key importance in understanding severe accidents and the capability of severe accident models to predict core damage progession leading to vessel failure. There are a number of uncertainties involved with the mechanisms of this relocation. The debris configuration, debris heat transfer properties, and vessel wall mechanical response to these severe conditions have not been clearly understood. This report focuses upon the questions involved with the vessel mechanical response: ultimate strength and creep behavior of the vessel. From this investigation the importance of vessel wall inner surface temperature magnitudes and the effect of accident temperatures on instrument assembly penetrations are assessed .

Heat transfer analyses have been performed using bounding assumptions in the lower head debris configuration and heat transfer properties between the debris and the vessel wall[1]. The upper bound thermal challenge to the vessel is postulated to result from a consolidated metallic/ceramic layer of core material adjacent to the vessel wall. The lower bound thermal challenge is envisioned to result from a porous debris bed separated from the vessel wall by a layer of non-fuel structural material. An intermediate level of thermal challenge is considered to result from a porous debris bed resting directly upon the lower head. In addition to these debris bed configurations, assumptions in debris coolability in the presence of operating system coolant have also been made. Assumptions of dry debris cooling as well as quenching by reactor coolant have been made for each of the debris bed configurations.

Simple calculations of stress based upon force equilibrium in the vessel wall indicated that some of the temperature distributions envisioned would cause vessel head failure based solely upon material ultimate strength at the indicated temperatures. This calculation considered the minimum pressure within the reactor vessel during the relocation temperature transient and the ultimate strength of the vessel material, which is a function of temperature. This observation showed that all of the assumed debris configurations with non-quenched cooling and the upper bound debris configuration with quenched cooling would fail the vessel. This failure would be caused by high temperatures lowering the vessel wall ultimate strength below stress levels caused by reactor system pressure. The remaining temperature scenarios to be investigated required more detailed analysis in which material creep properties were considered. The most severe of these was the intermediate quenched debris case, which was the one considered in this analysis.

The detailed structural analysis was performed using ABAQUS, a structural finite element code with geometric and material nonlinear capabilities. Time dependent system operating pressure was considered as well as the selected temperature history. Material creep behavior and ultimate strength properties were derived from data resulting from material tests performed up to 922K (1200°F)[2].

The calculated vessel wall maximum plastic and creep deformations were approximately 1% strain. These strains were not large, however, compared to test data indicating creep strains at rupture of about 35% and ultimate strength elongations of 25%[3]. This points out that even though temperature magnitudes were quite high on the inner surface of the wall (1300K), severe thermal damage in the form of material yielding and creeping was restricted to a rather localized area near the inner surface. The calculations indicate that the average vessel wall temperatures would not have resulted in significant creep during the selected temperature transient. Some redistribution of the loading from the region near the inner surface to the outer, cooler regions of the vessel wall did occur, however, causing plastic deformation on the outer surface of the wall and at points near the midsurface.

1.0 INTRODUCTION

The TMI-2 accident resulted in extensive core damage. The defueling effort of the reactor vessel by EG&G Idaho has shown that about 40% of the original core achieved melting temperatures and approximately 20 metric tons of molten core material relocated from the core region and settled on the lower head of the reactor pressure vessel (RPV)[1]. The high temperatures in the RPV wall resulting from this relocation have caused questions to be raised about the margin of safety between the actual accident conditions and those required to breach the vessel.

The usage of simplified methodology for answering these questions is preferrable since the information needed to calculate structural capacity of the vessel is not now, nor may ever be, well defined for TMI-2. However, simplification of a complex structural response requires assumptions and approximations which must be verified in order to provide a reasonable estimate of margin-to-failure for vessel rupture. The objectives of this investigation were to establish a method by which safety margin could be assessed, perform scoping calculations to provide insight into the mechanisms of failure and parameters critical to their cause, and provide some assessment of the validity of using simplified techniques for predicting safety margin of reactor vessels in such severe accidents.

Since the exact scenario of core relocation is not known, bounding assumptions were made in the finite element heat transfer analyses modeling the energy transfer from the molten debris to the vessel wall. The results of these bounding analyses were temperature distributions which could result from the various debris configurations and cooling assumptions. Some of these distributions were identified by simple analyses as being able to fail the vessel. The remaining ones required a more detailed evaluation for margin-to-failure determination.

Subsequently, a structural finite element stress analysis was performed considering: a plausible temperature distribution history, operating system pressure, material temperature-dependent plastic and creep properties, and nonlinear structural response. From this analysis, insight is offered upon the possible failure mechanisms and the appropriateness of simplifying assumptions for margin-to-failure determination. Additionally, areas of needed research for improved margin estimates are discussed.

Section 2.0 of this report describes the characteristics of the lower head of the RPV. Section 3.0 discusses the logic for determining margin-to-failure and for using the selected temperature distribution in the detailed analysis while Section 4.0 describes the heat transfer and structural modeling for this investigation. Section 5.0 provides results of the analysis and Section 6.0 draws conclusions and makes recommendations.

2.0 DESCRIPTION OF THE VESSEL LOWER HEAD

The TMI-2 RPV is a skirt supported vessel designed by Babcock and Wilcox. A cross section of the vessel arrangement is shown in Figure 1. The cylindrical portion of the RPV has an inner radius of 217 cm (85.5 in.) and a wall thickness of 24.1 cm (9.5 in.) while the spherical bottom head has an inner radius of 222 cm (87.25 in.) and a minimum wall thickness of 12.7 cm (5.0 in.). The skirt thickness is 5.1 cm (2.0 in.). The vessel has a stainless steel liner of 18-8 weld overlay with a nominal thickness of .48 cm (3/16-in.) and a minimum thickness of .32 cm (1/8-in.). The lower head contains 52 instrument penetration nozzles made of Inconel through which the in-core instrument assemblies access the reactor vessel.

The lower head is constructed of an axisymmetric forged section in the region of the vessel-skirt junction which is indicated in Figure 1. This forging is constructed of SA508-64, Class 2 material. The lower section of the head is constructed of SA533 Grade B, Class 1, plate material. A circumferential full penetration weld connects the forging to the plate section of the head near the shell-skirt junction. For this analysis, the debris was assumed to have settled uniformly on the bottom head. This limits the region of the vessel undergoing thermal attack to the bottom of the vessel, well away from the full penetration weld but in a region where numerous instrument assembly penetrations are located.

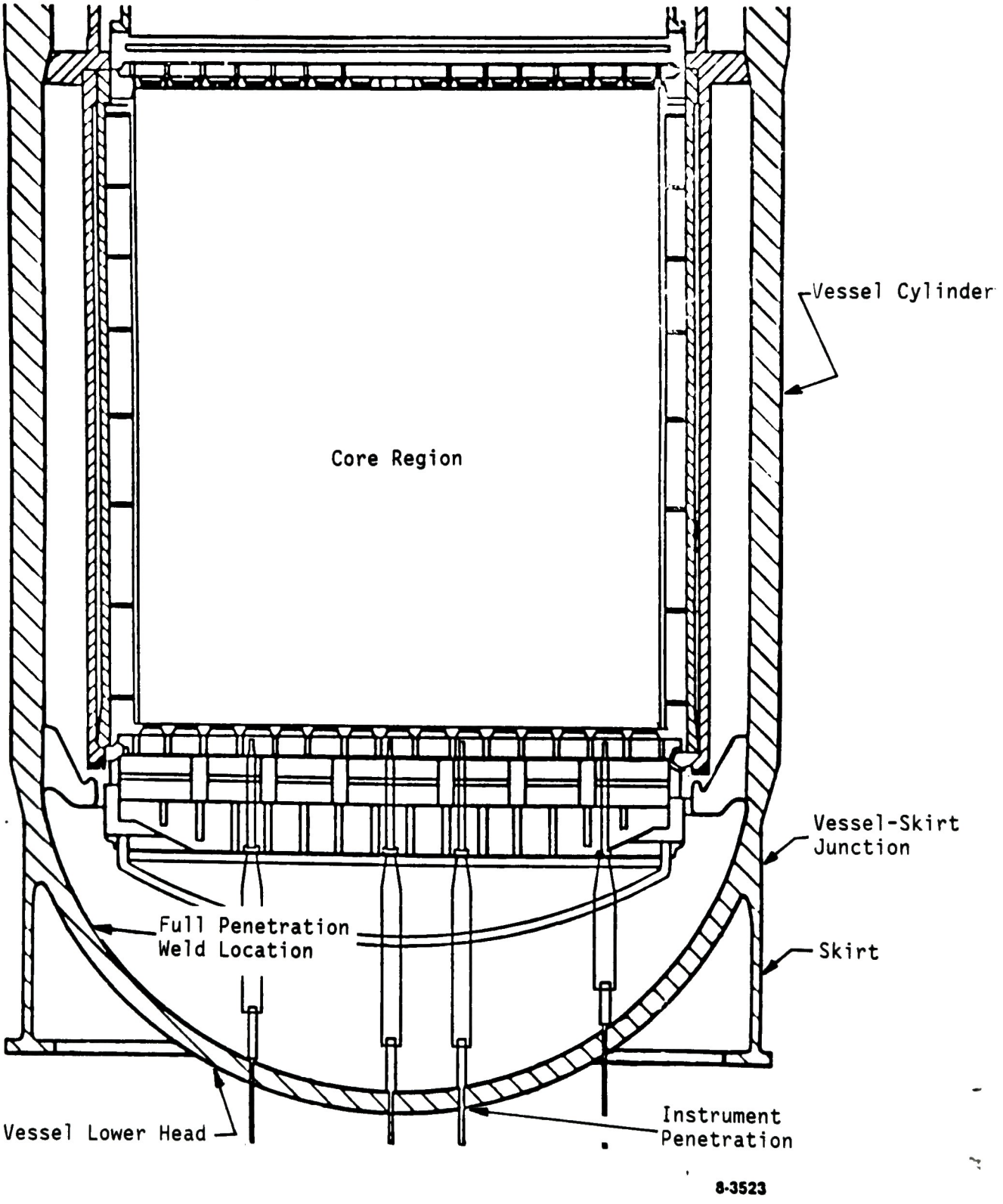

Figure 1. RPV Cross Section

3.0 DISCUSSION OF LOWER HEAD MARGIN-TO-FAILURE

Margin-to-failure determination requires knowledge of the vessel head's structural capacity and the loading actually applied to the head. Because of a lack of physical data on the debris bed and no measurements of vessel wall temperatures during the fuel relocation period, the thermal loading on the head was enveloped utilizing limited information known about the debris bed, assumptions in the character of the debris bed, and finite element heat transfer analyses. The mechanical loads were limited to operating system pressure, which was monitored during the relocation. Material properties are not completely defined for temperatures in the upper bound temperature profile. Therefore, estimates in properties were made in the structural finite element models in order to determine vessel capacity.

The following subsections describe the thermal and mechanical loading and discuss the method for making initial estimates of capacity and subsequent selection of temperature profiles for refinement of these estimates by using a structural finite element model.

3.1 Bounding Vessel Wall Thermal Histories

A lack of physical data on the lower head debris bed has caused uncertainty in the understanding of the actual rate of heat transfer from the debris to the vessel wall. This affects the wall temperature distribution calculated in the heat transfer analysis and its subsequent effect upon the vessel head's structural analysis. Therefore, a study aimed at bounding the possible vessel thermal response has postulated three debris bed configurations as shown in Figure 2. This study was based upon information from the preliminary inspection of the debris bed.

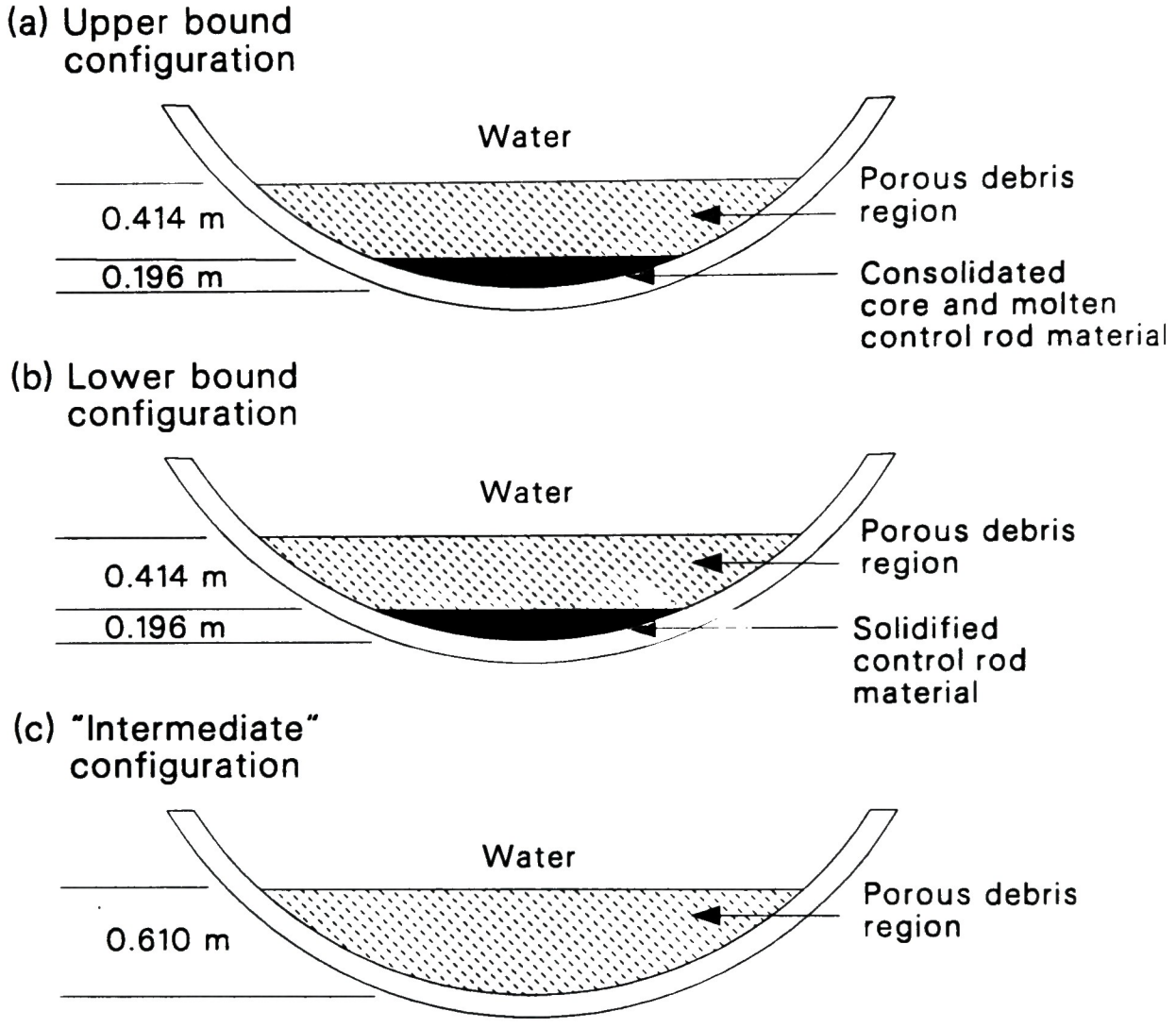

P707 GLT-888-01

Figure 2. Bounding Debris Configurations

Figure 2(a) illustrates the debris bed configuration thought to result in an upper bound thermal load in the vessel wall. This consists of a porous debris bed with regions adjacent to the vessel wall having interstices filled with molten control rod material, resulting in a consolidated metallic/ceramic sublayer. This sublayer is assumed to transmit heat to the vessel wall very rapidly. The lower bound case shown in Figure 2(b) is assumed to consist of a layer of solidified control rod material adjacent to the vessel wall which had relocated prior to the major core relocation. This layer was then covered with porous debris from the core. In this case, the layer of solidified control rod material acts as a heat sink and additional thermal resistance to heat transfer between the debris and the vessel wall.

The cooling of the debris and transfer of heat to the lower plenum coolant is another important uncertainty. Debris cooling was estimated in the calculations by bounding assumptions on the heat transfer and quenching rates of the debris. An upper bound on the rate of debris cooling was assumed to result from water penetration into the debris bed and resulted in cooling of the debris within 20 minutes. A lower bound assumption on the rate of debris cooling assumed no water penetration into the debris bed, thus limiting heat transfer from the debris to: conduction through the debris, surface convection to the coolant at the upper debris surface, and convection and conduction to the vessel wall at the debris/vessel interface.

Figure 3 illustrates the results of the heat transfer analyses. The inside vessel wall temperatures, labeled "I.S.", and outside wall temperatures, "O.S.", are indicated. The vessel wall temperatures for the assumption of no liquid penetration and quenching of the porous debris, are shown as solid lines while the temperatures assuming quenching of the porous debris are denoted by dashed lines.

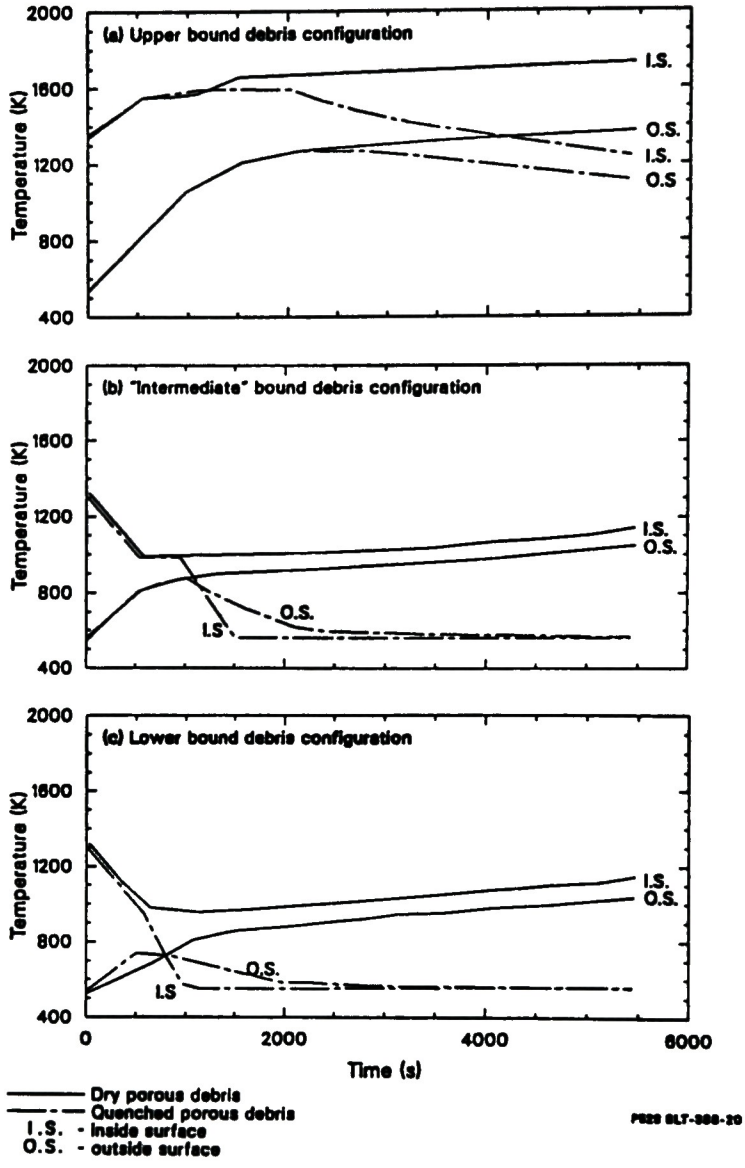

Figure 3. Calculated Temperature Gradients for Bounding Debris Configurations

3.2 Mechanical Loads

Figure 4 shows the variation in the operating system pressure during and after the relocation. This pressure, which was monitored by pressure transducers during the accident, was the major contributor to the mechanical loads on the lower head. The combined pressure on the lower head resulting from water in the RPV and the weight of the core material distributed over the lower head amounted to about .07-.14 MPa (10-20 psi) compared to operating system pressures as high as 11 MPa (1600 psi) during the relocation period. The weight of the reactor vessel is transferred through the cylindrical portion of the RPV down to the skirt support which is well away from the high temperature region. Therefore, the system transient pressure was the only significant force causing primary stress in the lower head.

This type of stress is not self-limiting, i.e., it does not reach a limit as strains increase. Therefore, this load must always be carried by the lower head vessel wall to maintain structural integrity of the RPV. A simple calculation of the tangential stress in the lower head, a uniform stress through the wall resulting from the system pressure, indicates a minimum stress resulting from system pressure during the transient of 74 MPa (11 ksi).

3.3 Vessel Margin-to-Failure

The effects of creep on a structure's capacity are quite complex and not easily determined when temperatures are not uniformly distributed throughout the structure. This structural characteristic accompanies the material's ultimate strength at temperatures above 700°F for carbon steels such as is found in RPV's. However, since ultimate strength is a temperature-dependent but not a time-dependent material characteristic as is creep, it can be used to screen some temperature distributions out of the list of possibilities, considering that the vessel capacity was not exceeded during the accident.

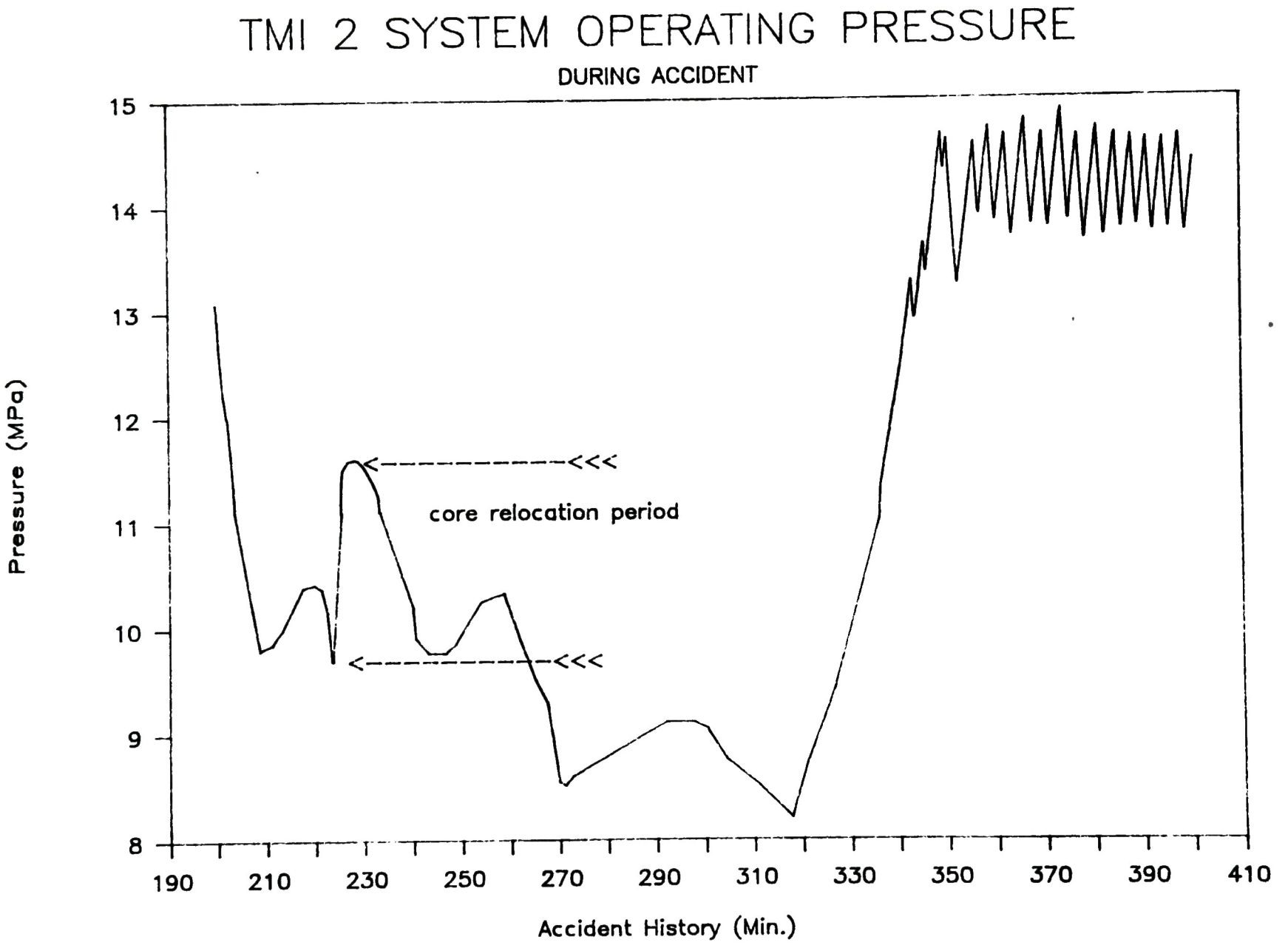

Figure 4. Measured TMI-2 Reactor System Pressure
During the Core Relocation and Associated Thermal Transient

Inspection of Figures 3(a), 3(b), and 3(c) shows the dry cooling assumption in each debris configuration causes temperature distributions through the wall whose average temperatures trend linearly upward beyond 2000 s after the core relocation. If one extends the ultimate strength curve of SA533 Grade B Class 1, the material in the vessel wall under the settled debris, the ultimate strength is approximately 69 MPa (10 ksi)[2] at 1144K. This is about the minimum stress induced in the vessel wall by operating pressure during the early stages of the relocation when the vessel wall temperatures would be highest. As can be seen in Figure 3, the temperature distributions resulting from the dry debris cooling for all of the configurations either exceed this temperature throughout the wall within the first 2000 s of the transient, as in the case of the upper bound, or indicates a trend in which minimum wall temperatures would exceed 1144K within 7000 s of the transient in the intermediate and lower bound debris configurations. This would indicate that the dry porous debris cooling assumptions do not appear to be credible without a vessel breach, which does not appear to have happened. By the same reasoning, the upper bound configuration with quenched porous debris cooling would also have low probability of occurrence.

This essentially leaves the intermediate and lower bound configurations with the quenched porous debris cooling assumption being the more probable temperature scenarios. In both cases, the inside temperature would be temporarily high enough to reduce the ultimate strength on the inside below expected pressure stresses; however, the outside temperatures would be low enough that ultimate strength could easily exceed expected primary stresses. Therefore, these scenarios could not be screened out for having low probability of occurrence in the simplistic manner discussed above. Thus, these scenarios were ones requiring closer scrutiny with a detailed structural model.

4.0 MODELING OF THE DEBRIS HEAT TRANSFER AND THE VESSEL WALL STRUCTURAL RESPONSE

The screening process was performed to focus on the more probable temperature histories in the accident. The gross assumption of neglecting the effects of thermal bending in the wall did not allow a determination with high certainty of the possible failure modes of the accident. It only produced a place to start the analysis. By use of the detailed stress analysis, insight into the effects of thermal bending, creep, and plasticity was anticipated.

The intermediate level debris configuration was chosen as the transient to investigate since it was the more stringent of the two remaining plausible transients when vessel creep response was considered.

4.1 Heat Transfer Model

Figure 5 shows a schematic of the axisymmetric finite element heat transfer model of the lower head and relocated core material. The illustration indicates locations, or stations, along a meridian of the lower head for which radial temperature distributions are defined for the structural model of the lower head. This particular model is a modification of the original model by Moore[1] using the COUPLE/FLUID[4] finite element code to provide a radial temperature distribution at five points through the wall corresponding to nodal locations on the structural model. This heat transfer code solves the two dimensional energy transport equation using quadratic elements.

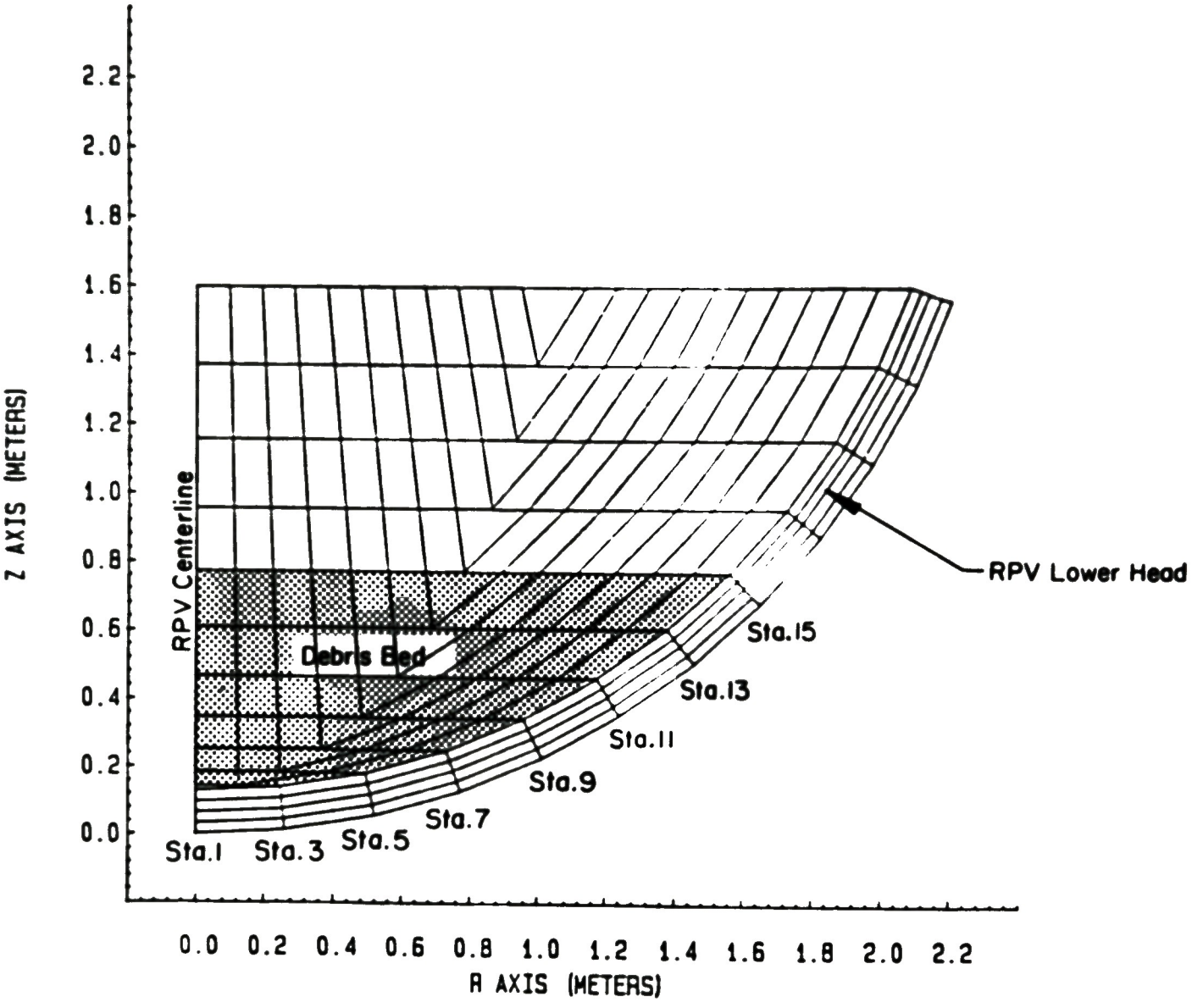

Figure 5. COUPLE Finite Element Model of TMI-2
Lower Head Debris and Vessel Wall

The heat transfer model of the debris and lower head of the vessel assumes axisymmetric behavior around the RPV centerline and consists of a porous debris region of 121 elements and a vessel wall region of 44 elements. The outer surface of the vessel wall simulated heat transfer through the thermal shield to the interior of the RPV support pedestal. The containment temperature was assumed to be 311K (100°F) and the initial temperature of the head was 559K (547°F) while the initial debris temperature was assumed to be 2500 K (4040°F). A quench time of 20 min was used and the quench front was assumed to move radially from the outer edge of the debris bed towards the vessel centerline. A constant energy removal rate from the debris was assumed to determine the radial quench front location with respect to time for the analysis.

Figures 6 through 11 plot the temperature histories at the five radial points through the wall at stations 1, 2, 3, 13, 14, and 15 with inner surface temperatures being initially hottest. These temperature histories correspond to the analysis of the intermediate level debris configuration with quenched cooling. The quench front, i.e., the cooling wave moving from the edge of the debris to the centerline of the vessel, is represented in Figures 6 through 11 by the abrupt drop in inner surface temperature. The first three stations (indicated on Figure 5) range from the RPV centerline outward while the last three stations show temperature distributions near the outer edge of the relocated debris. Stations 4 through 12 are not plotted but offer intermediate values in temperatures and quench front times. The rest of the structure was assumed to remain at a constant temperature of 559K throughout the structural analysis.

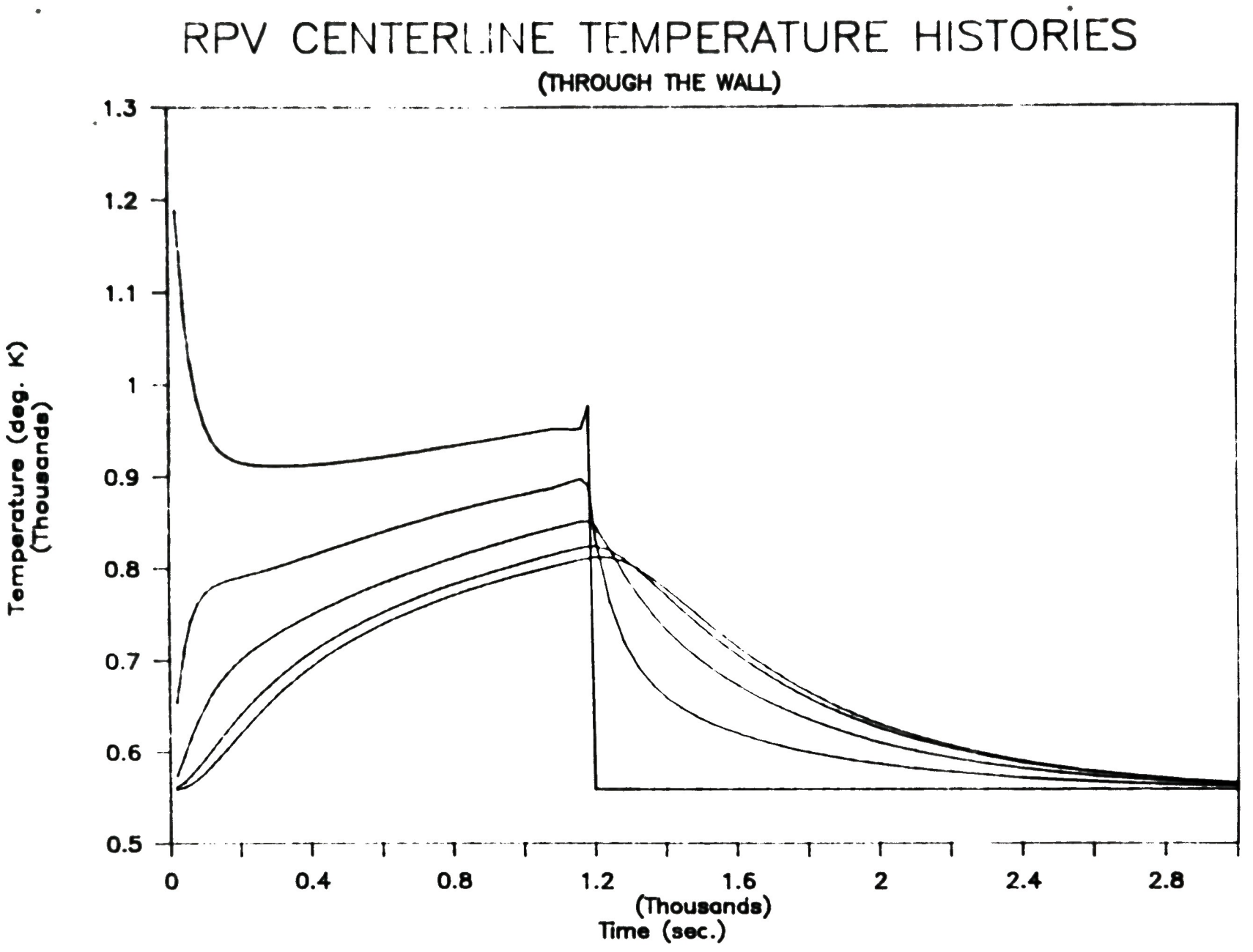

Figure 6. RPV Centerline Temperature Histories

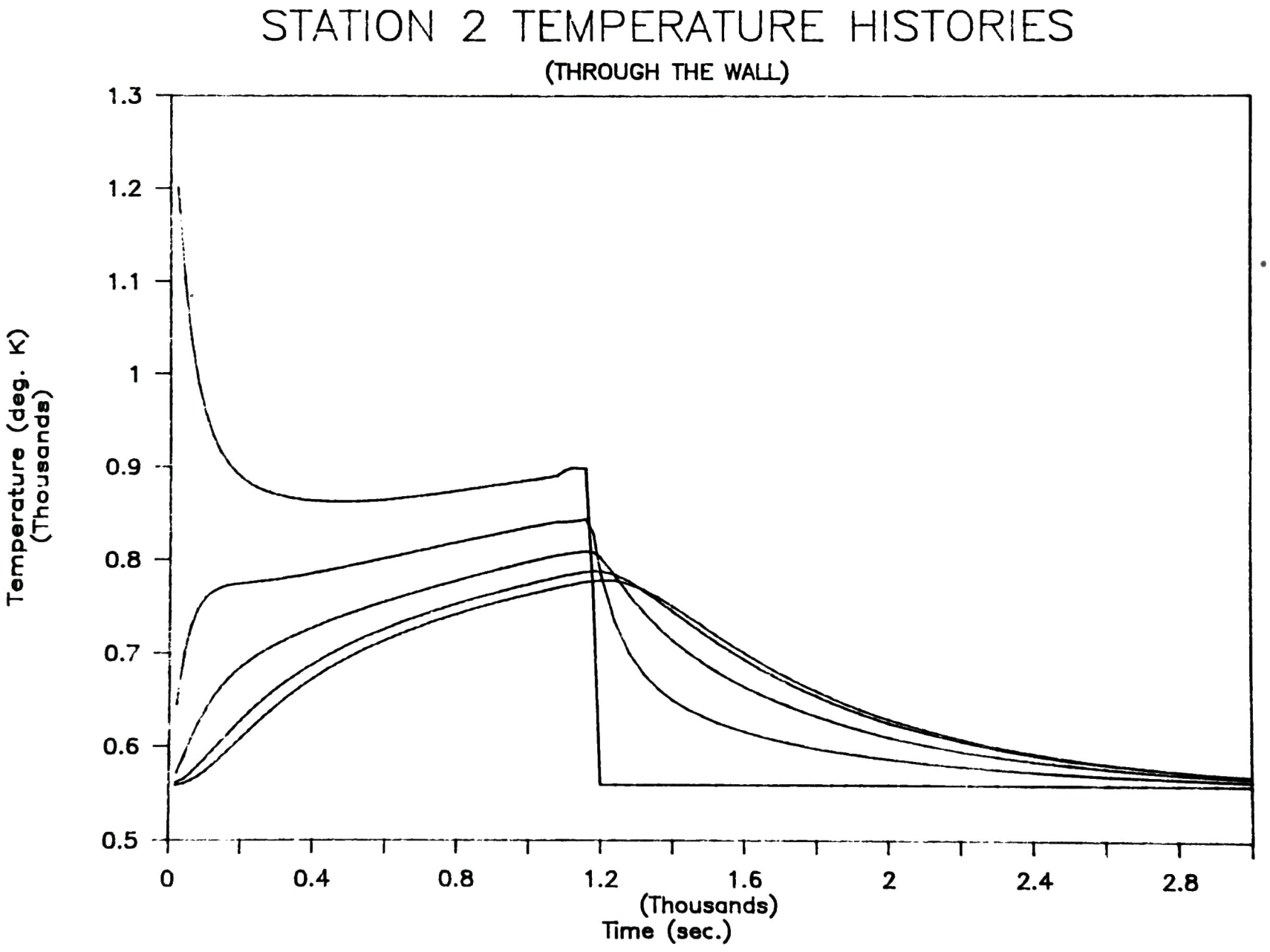
STATION 2 TEMPERATURE HISTORIES
(THROUGH THE WALL)
Temperature (deg. K)
(Thousands)
1.3
1.2
1.1
1
0.9
0.8
0.7
0.6
0.5
0
0.4
0.8
1.2
1.6
2
2.4
2.8
(Thousands)
Time (sec.)

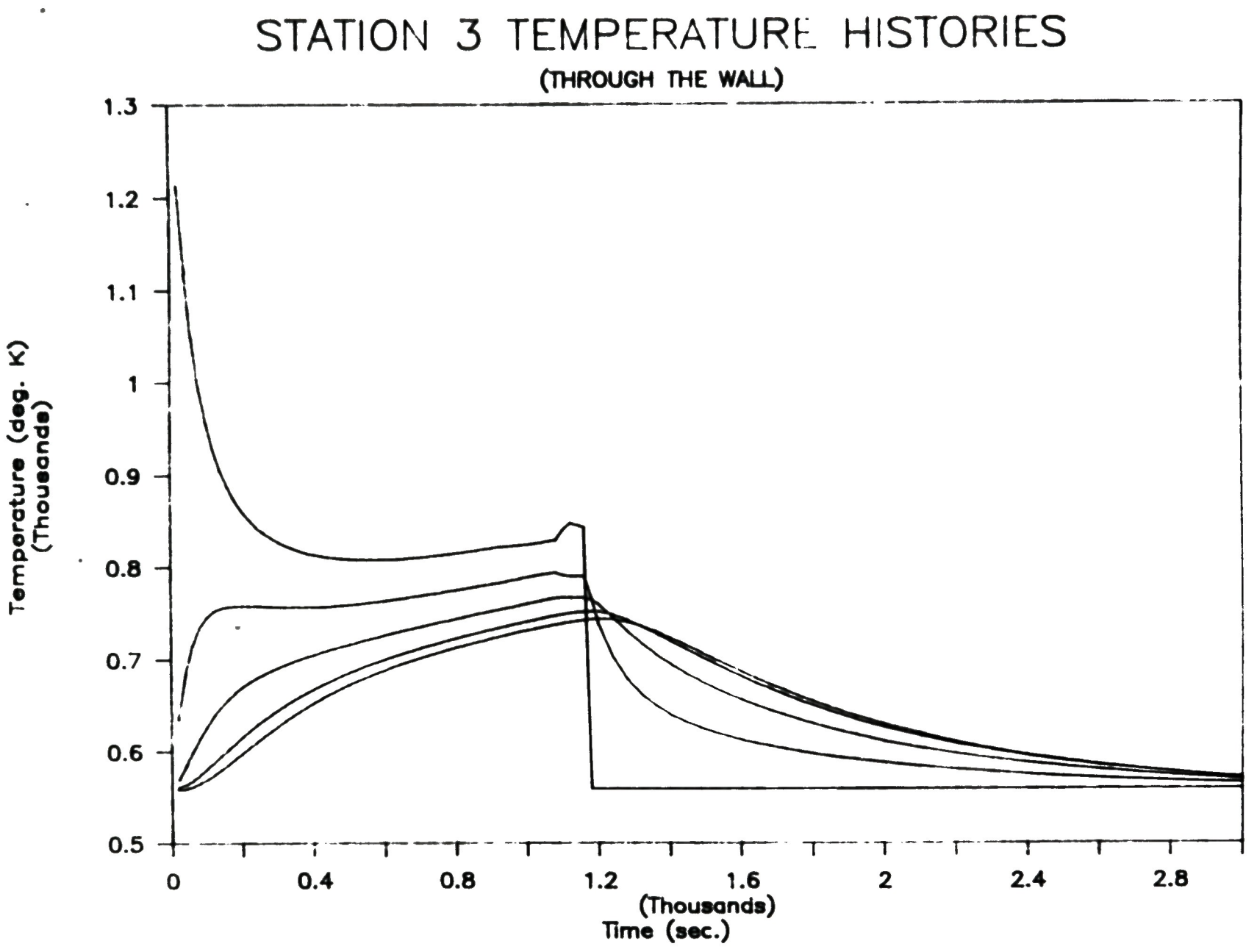

Figure 8. Station 3 Temperature Histories

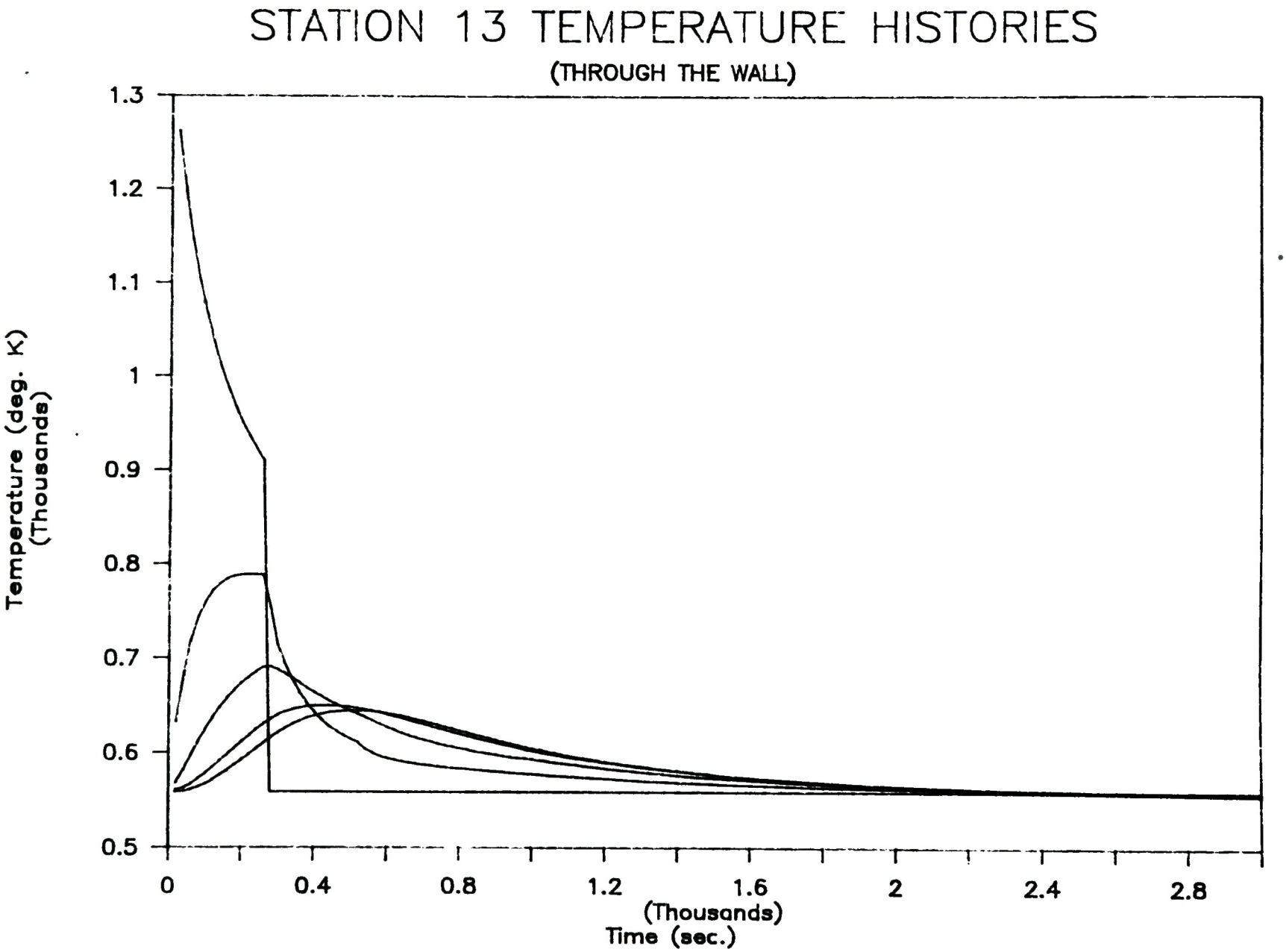
STATION 13 TEMPERATURE HISTORIES
(THROUGH THE WALL)
Temperature (deg. K)
(Thousands)
1.3
1.2
1.1
1
0.9
0.8
0.7
0.6
0.5
0
0.4
0.8
1.2
1.6
2
2.4
2.8
(Thousands)
Time (sec.)

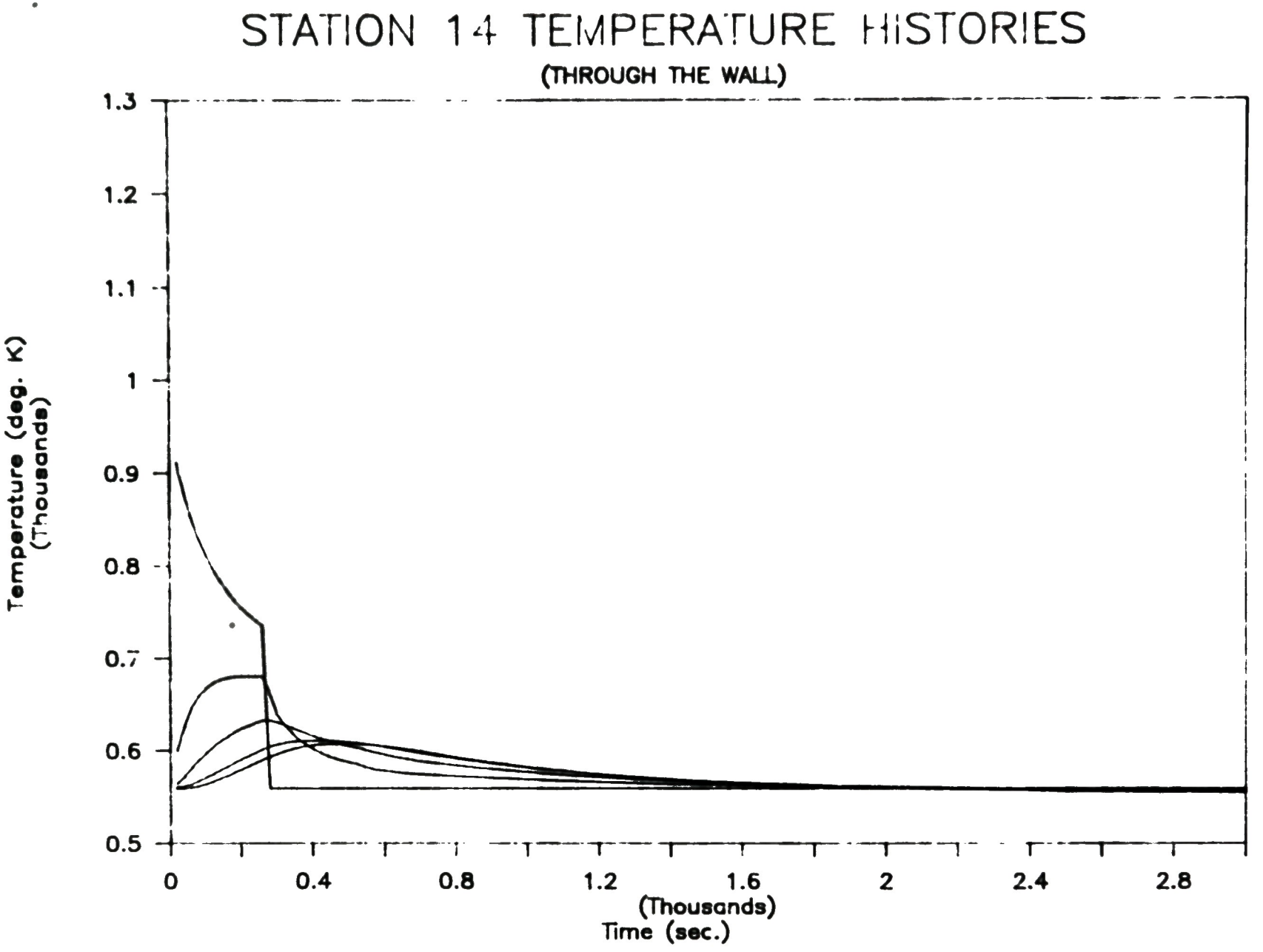

Figure 10. Station 14 Temperature Histories

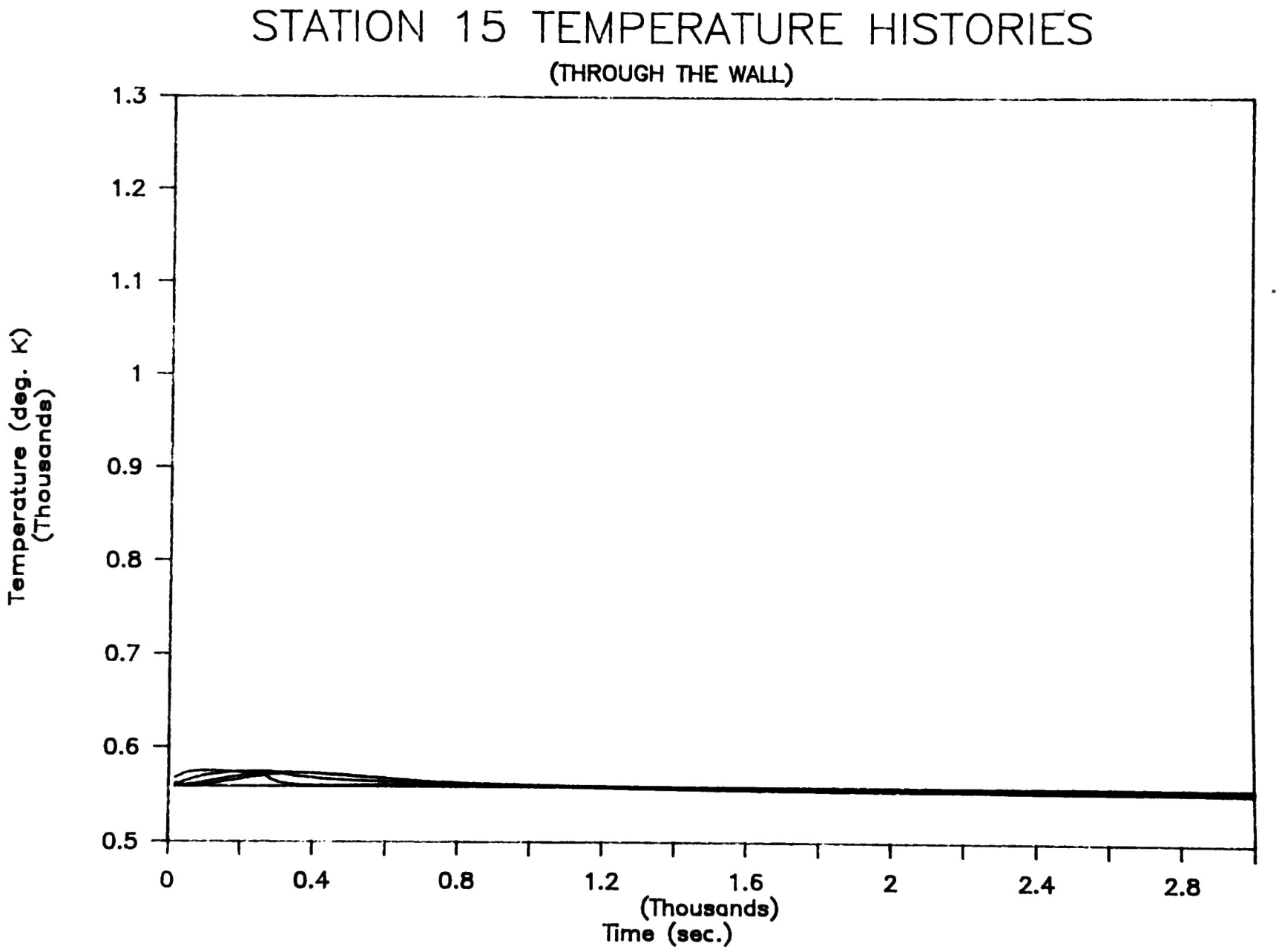
STATION 15 TEMPERATURE HISTORIES
(THROUGH THE WALL)
Temperature (deg. K)
(Thousands)
1.3
1.2
1.1
1
0.9
0.8
0.7
0.6
0.5
0
0.4
0.8
1.2
1.6
2
2.4
2.8
(Thousands)
Time (sec.)

4.2 Structural Model

An axisymmetric model of the lower head, skirt, and a cylindrical portion of the RPV was made using the ABAQUS[5] nonlinear structural finite element code. An eight node, axisymmetric continuum element, the ABAQUS CAX8 element, was the primary element used in the model. This element uses a biquadratic interpolation with 3 x 3 integration. The CAX6 element, a six node version of the continuum element, was used in the model where triangular elements were required. The model is shown in Figure 12. The critical portion of the model, the spherical head region below the skirt junction, was modeled with two elements through the thickness and ten along the meridian of the lower head up to the skirt junction. Symmetrical boundary conditions (fixed horizontal translation) were applied at the RPV centerline degrees of freedom while boundary conditions of continuity (fixed vertical translation) at the degrees of freedom on the cylindrical portion of the RPV axisymmetric model were imposed.

Since the scope of this analysis was limited to an axisymmetric response of the lower head to the core relocation, the plate material, SA533, Grade B Class 1, was the primary material of concern. High-temperature elastic-plastic and creep properties for SA533 Grade B, Class 1 material have been documented by Reddy and Ayres[3] from tests performed up to 922K (1200°F). Such properties beyond this temperature are not available at this time. The ABAQUS model uses the 922K properties for any higher temperatures encountered at the element integration points.

Appendix A contains plots of the following data at various temperatures up to 922K (1200°F) as extracted from Reference 3: stress-strain curves, Young's modulus and proportional limit stresses, and material creep properties. Also included in this appendix are mean coefficients of thermal expansion as derived from this reference and used in the analysis.

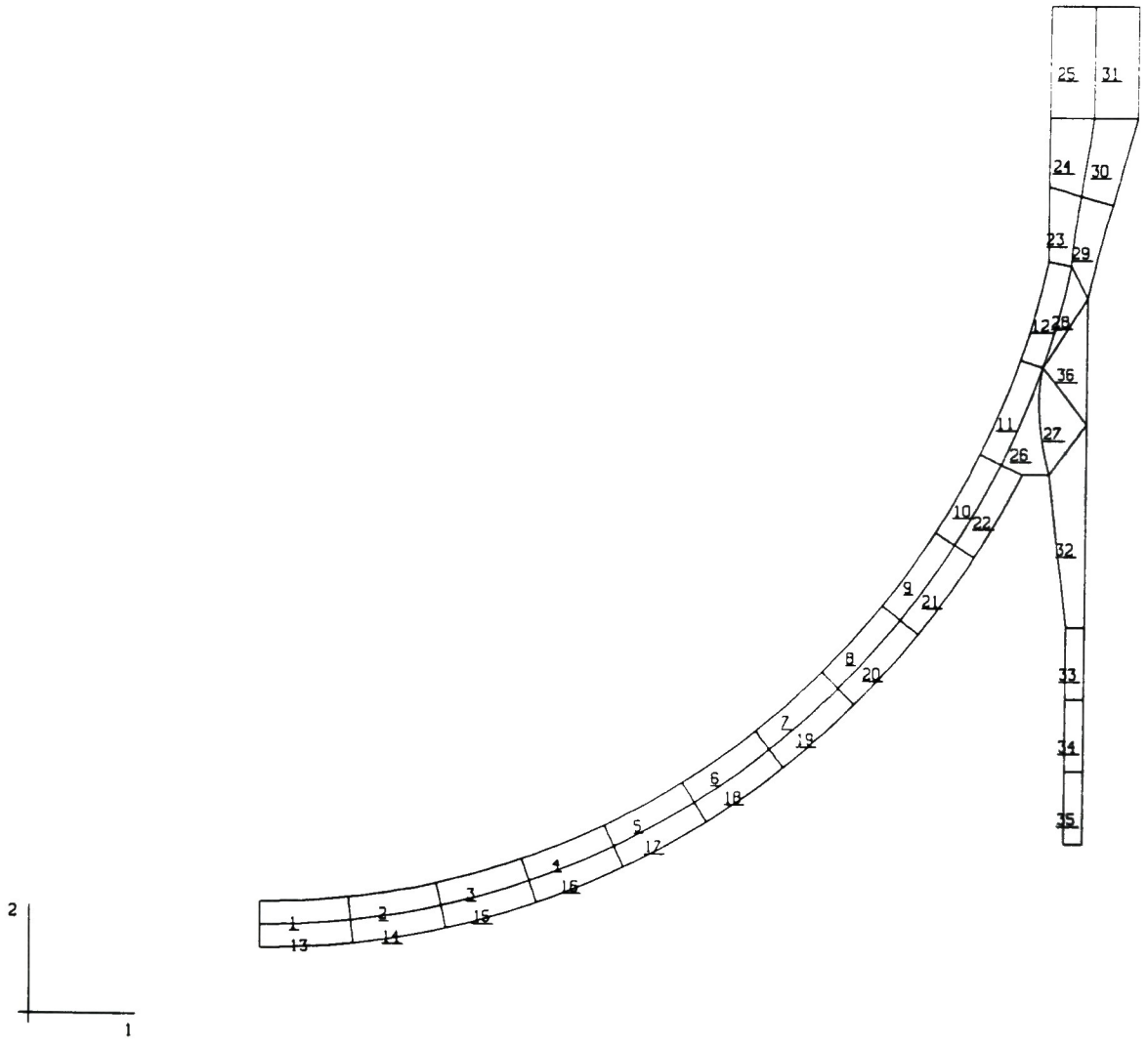

Figure 12. TMI-2 Lower Head Structural Model

The creep strain plots from Reference 3 compare test data with an analytical constitutive equation developed to represent that test data. That equation relates creep strain to temperature, effective stress, and time in the following general form:

$$(1) \qquad \epsilon_c = A^B \left(\frac{\sigma}{\sigma_m}\right)^C t^B$$

where: ϵ_c = creep strain

A, B, and C = functions of temperature

t = creep time

σ = effective stress

σ_m = function of effective stress and temperature.

The actual form of the equation and its associated parameters as stated in the reference are also listed in Appendix A. Inspection of these comparison plots show that the actual test data for the higher temperatures was limited to smaller stress ranges. As will be discussed later in more detail, some effective stresses encountered in the TMI-2 analysis were beyond these stress ranges and the constitutive law was used as an extrapolation to this test data to approximate creep strains at the higher stresses.

ABAQUS provides the option of either using a creep law supplied directly in the ABAQUS coding or a user-supplied creep law subroutine. For this analysis, the ABAQUS creep law was used and, even though of slightly different form, was typically within about 10% of the creep strain calculated by Equation (1) when appropriate parameters were used. This was acceptable for these scoping calculations. The ABAQUS creep law (in time hardening form) is as follows:

(2) $$\epsilon_c = \frac{A}{m+1} \sigma^n t^{m+1}$$

where: ϵ_c = creep strain

A, m, n = functions of temperature

σ = effective stress

t = creep time

Comparison of Equations (1) and (2) show them to be quite similar in general form with the exception of the variable σ_m in equation (1) which is jointly dependent upon effective stress, σ, and temperature. However, by adjusting the temperature dependent parameters at discrete temperatures of 672K (750°F), 755K (900°F), 839K (1050°F), and 922K (1200°F) and at discrete effective stresses corresponding to those of the test data of Reference 3, plots of Equations (1) and (2) agree quite well. Figure 13 shows a comparison of the two equations at 839K and effective stresses of 68.95 MPa (10 ksi), 137.9 MPa (20 ksi), and 206.35 MPa (30 ksi).

In actuality, ABAQUS cannot use the creep law in the form of (2) but must formulate the law into an incremental form. This is done by first determining the creep rate from (2):

(3) $$\frac{d\epsilon_c}{dt} = A \sigma^n t^m$$

and then expressing the creep in incremental form:

(4) $$\Delta\epsilon_c = A \sigma^n t^m \Delta t$$

where: t = creep time

Δt = time step

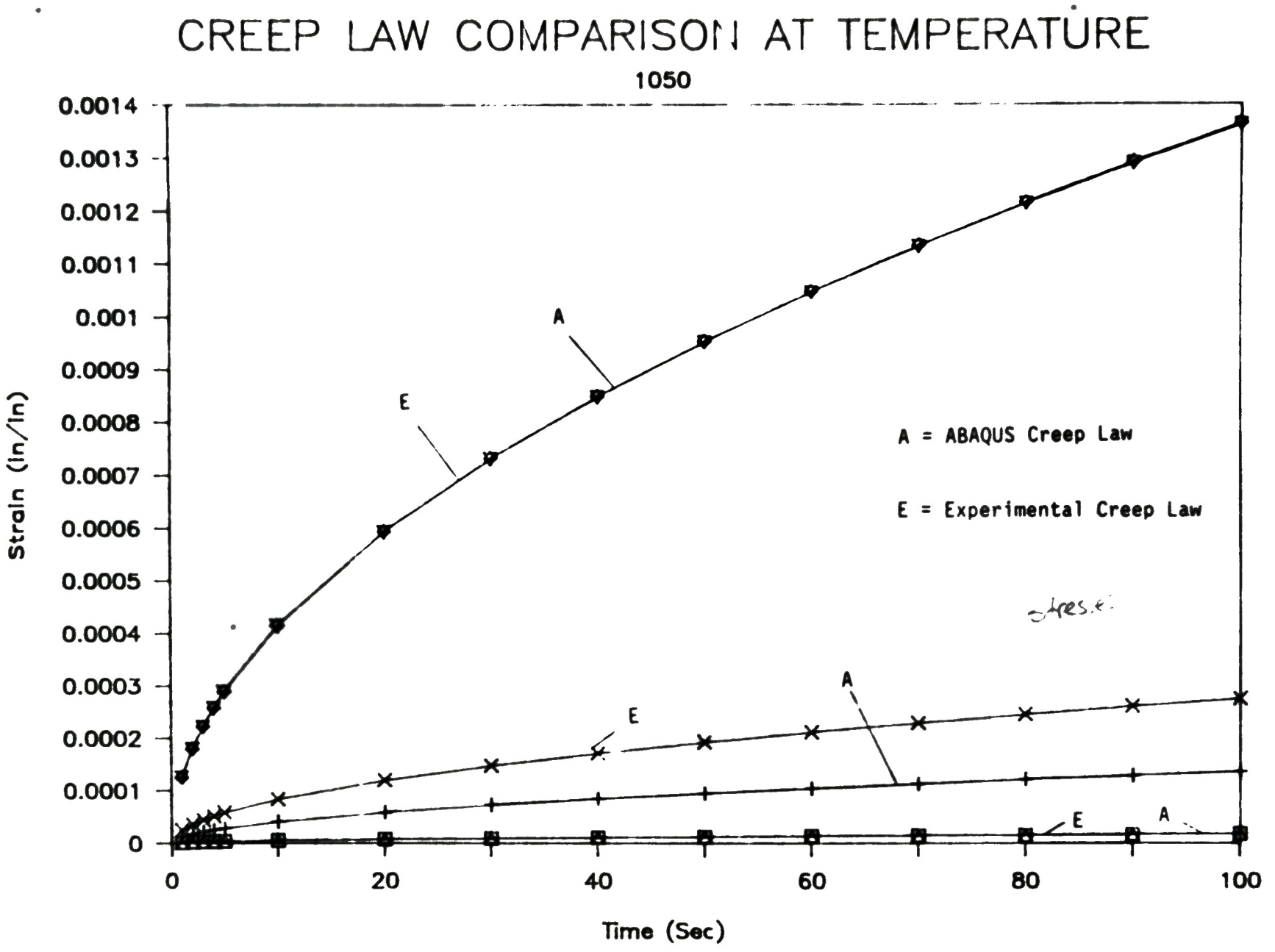

Figure 13. Creep Law Comparison at Temperature 839K (1050°F)

In creep analyses, there are two generally accepted forms of the creep law. The first is the time hardening form as shown in (3) where creep strain rate is expressed as a function of temperature, stress, and time. The second and more widely accepted form, called the strain hardening form, expresses creep strain rate as a function of temperature, stress, and accumulated creep strain. The strain hardening form is developed by solving for t in (2) and substituting that result into (3). The strain hardening form of the creep law was used in this analysis.

The temperature dependent stress-strain curves of Reference 3 which are illustrated in Appendix A were used in the model in tabular form. In the same manner, the temperature dependent mean coefficients of thermal expansion, Young's moduli, and yield stresses were also tabulated in the model. ABAQUS interpolates between these discrete tabulations to arrive at the various parameters, as needed, during the thermal time history analysis.

As was discussed in Section 3.0, time varying temperatures were applied at all nodes in the vessel wall in the debris region of the structural model. The remainder of the model nodes were kept at a constant 560K (547°F).

Since isoparametric finite elements were used in this analysis, elemental properties are determined as a function of element integration point temperatures. These temperatures are determined via an interpolation, or shape, function which is dependent upon the chosen element type. A quadratic polynomial is used to interpolate nodal temperatures of each element to get integration point temperatures. This interpolation causes a significant difference between the inner wall nodal temperatures and the inner most integration point temperatures in the structural elements. This seems justifiable since, for the given temperature scenario, the extreme temperatures are highly localized in the region of the inner surface of the vessel wall. Thus, the affected region

would load up, stress relieve, and redistribute load on the inner elements in a smoothing manner similar to the effect of interpolation. This is an approximation which seems appropriate since increased accuracy of the temperature representation at the elemental level would require a very large increase in model size. As a result of this temperature interpolation, maximum integration point temperatures encountered in the structural model were approximately 1000K (1340°F) which is only slightly higher than temperatures for which material creep and ultimate strength test data are available.

In addition to the temperature loading, the reactor system operating pressure time history of Figure 4 was applied at all elements on the inside surface of the structural model. This pressure ranged from a maximum of 11.6 mPa (1683 psi) to a minimum of 9.7 mPa (1406 psi) during the analysis.

The structural analysis was broken into three sequential steps. The first step brought the structure to a static equilibrium state at 9.7 MPa (1407 psi) internal pressure and a uniform temperature of 559K (547°F). There was no nonlinear structural behavior during this step. These were the conditions prior to the relocation transient. This condition produced an average effective stress (von Mises stress) in the wall of 86.9 MPa (12.6 ksi) which agreed with the calculation:

(5) $$\sigma = \frac{pr}{2t}$$

where: σ = tangential stress in a sphere
p = internal pressure
r = mean radius of the sphere
t = wall thickness

This stress changed very little throughout the region of the model under the debris indicating very little influence resulting from boundary effects in this critical region for uniform pressure loading.

The second step of the analysis kept the internal pressure loading at a constant 9.7 MPa but increased nodal temperatures in the vessel wall under the debris to the initial values of the temperature transient which is partially illustrated in Figures 6 to 11. The structural model incurred plastic deformation but had no material (time-dependent) creep properties in this step.

The third and final step utilized the end state of the second step for initial conditions and added material creep properties to the structural model. This third step analyzed the time-dependent nonlinear structural response of the lower head to the internal pressure loading exhibited in Figure 4 and the nodal temperature histories exemplified in Figures 6 to 11. This analytical step extended over the first 1600 s of the loading transients.

5.0 RESULTS

The results of the creep analysis are summarized by the through-wall stress gradients in Figures 14 and 15. Both plot the tangential stress component gradients of all three analysis steps described in Section 5.0. Stresses are plotted at integration points distributed radially through the wall thickness. Figure 14 plots the stress distribution through the wall near the RPV centerline and Figure 15 plots the distribution closer to the edge of the debris bed at station 11 as designated in Figure 5. Step 1, the elastic step, is designated as "S1" while step 2, the elastic-plastic step, is labeled "S2". The gradients from the elastic-plastic-creep portion, step 3, are plotted from response stress components at various times throughout this step. Each gradient in this step is labeled with the time in seconds of the visco-elastic analysis at which the gradient occurred. Only one of the tangential stresses was plotted because both components were approximately equal throughout the analysis. Integration point stresses which indicated yielding in step 2 are labeled with a "Y" while integration points in step 3, which indicated plastic response occurring at the time of the gradient, are designated with an "AY" (actively yielding).

Inspection of these two figures shows that the stress gradient throughout the accident is dominated by the temperature effects even though the maximum integration point temperature was only about 1000K (1350°F). Comparison of the pressure stress gradient, "S1", in each location with the subsequent stress gradients illustrates this point. Step 2 resulted in a high thermal bending stress gradient which produced yielding throughout a major portion of the inner half of the vessel wall. As the analysis proceeded through step 3, creep relaxation of the inner surface stresses caused a redistribution of the load to the center and outer portions of the wall. Enough of the load was shifted to the outer portion of the wall to achieve some plasticity at the outer surface. Once the outer surface yielded, the load was again redistributed so that the middle portion of the wall temporarily carried more of the load. However,

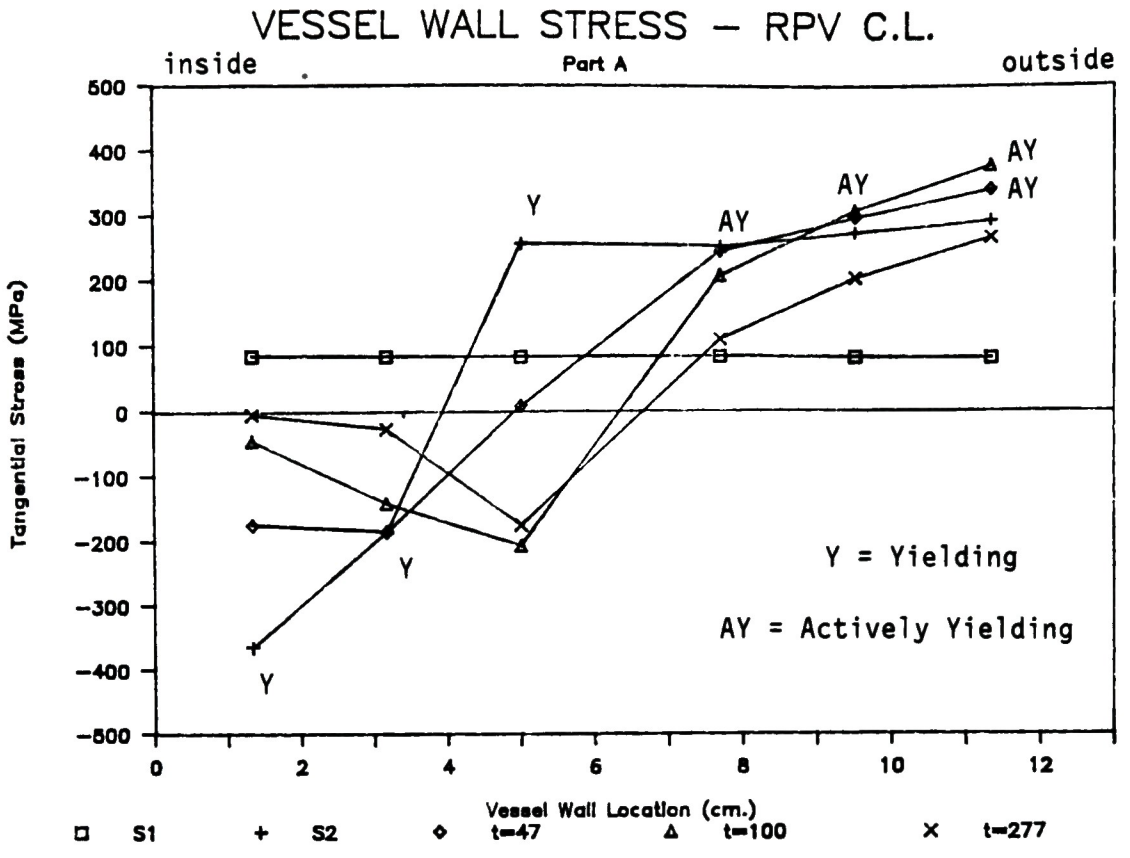

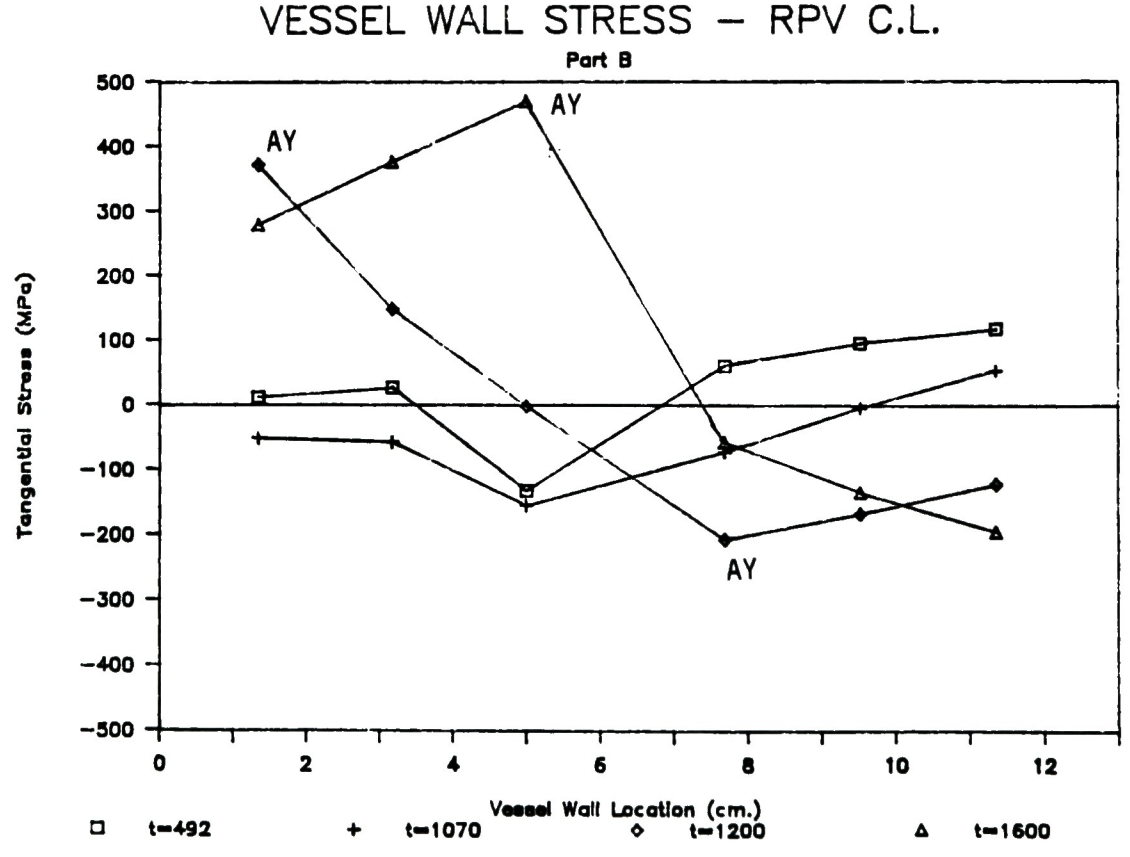

Figure 14. RPV Wall Tangential Stress Distributions at the Vessel Centerline

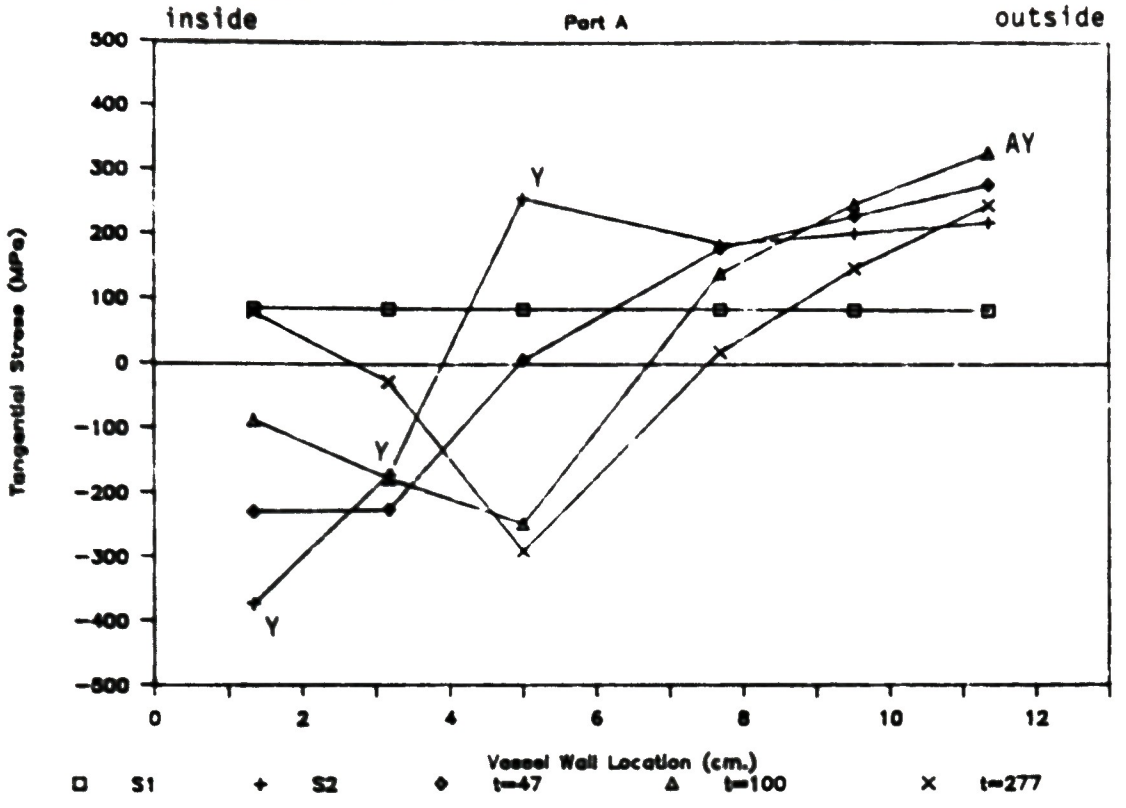

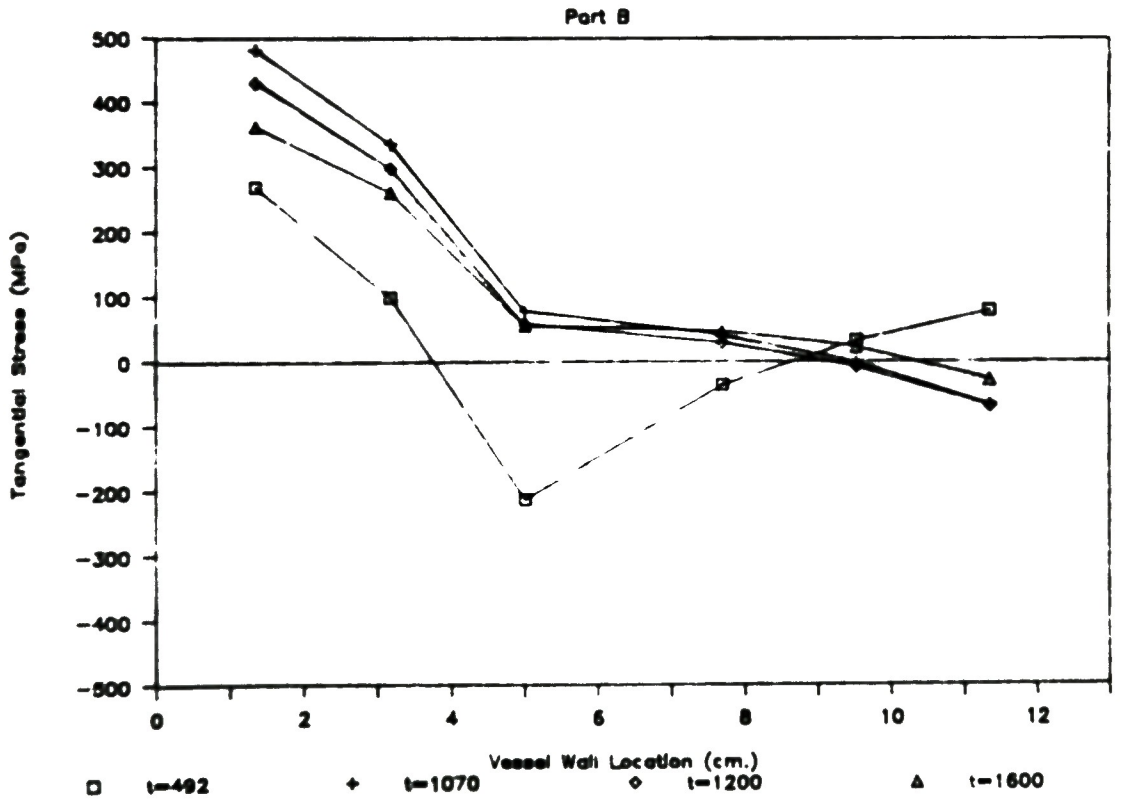

Figure 15. RPV Wall Tangential Stress Distributions at Station 11

by this time ($t \geq 277$ s) the temperature difference across the wall at all locations under the debris had reduced significantly and the quenching effects from the wall sections out at the edge of the debris bed started to take effect. This resulted in temporary compressive stress across most of the wall thickness at the RPV centerline at a time of 1070 s. At the same time, a general reversal of the thermal stress gradient (from the initial condition of step 2) occurred as the quench front moved from the outer edge of the debris towards the RPV centerline. After this reversal, the same process of load redistribution occurred as it had before. The inner surface wall stresses creep relieved in wall sections ahead of the quench front and redistributed the load to the center and outer portions of these sections. Some yielding, even in the center portion, resulted from this redistribution as seen at a time of 1600 s at the RPV centerline. Wall sections through which the quench front had already passed did not creep relieve because of the lower temperatures but the thermal stress gradient reduced as the temperature difference through the wall reduced at the RPV centerline.

Even though yielding did occur at various times at locations distributed throughout the wall thickness, the inelastic deformations were rather small. Maximum elastic strains, including thermal expansion, were of the order of 2% while maximum plastic and creep strains were each approximately 1%.

From this picture of the structural response to the given temperature history, a list of critical parameters to the severity of stress in the wall can be made. They are as follows:

1. Thermal conductivity through the vessel wall
2. Heat capacity of the material
3. Quench front velocity
4. Contact temperatures

5. Creep and plasticity properties of the wall material above 922K (1200°F)
6. Creep properties in the 672K (750°F) to 922K at high stress.

The first four parameters affect the severity of the thermal loading while the last two affect severity of material deformation.

6.0 CONCLUSIONS AND RECOMMENDATIONS

The state of stress through the vessel wall is quite complicated. The overall stress gradients are dominated by the thermal gradients in the vessel wall under the debris bed. Plastic and creep deformations occur causing redistribution of stress throughout the wall thickness. Stress gradients also undergo reversals over the life of the transient. Plastic deformations occur at various locations throughout the wall thickness at various times during the transients. Both compressive and tensile yielding occur on the inner half of the wall while primarily tensile yielding is exhibited in the outer portion. Even though plastic deformation was widely distributed, it was not very high. Maximum plastic and creep strains were each in the 1% range. Reference 3 reports creep rupture strains at 783K (950°F) of about 35% and elongations at ultimate strength and 783K (950°F) of about 25%.

Inelastic material test data for SA533 Grade B Class 1 material are presently only available for temperatures up to 922K. This transient had a brief period in which a highly localized portion of the vessel wall inner surface experienced temperatures as high as 1255K (1800°F). Because of the elemental shape functions, the highest integration point temperatures were about 1000K (1350°F). It is estimated that inclusion of these properties, if they were known for the higher temperatures, would increase plastic deformations in the majority of the wall only a minimal amount because of the highly localized distribution of these high temperatures.

The conclusion drawn from these scoping calculations is that rupture of the lower head resulting from large temperature differences across the vessel wall is not very probable. The temperature distribution used here restricts the high temperatures to the inside surface and the transient is really not long enough to mobilize any significant creep in the wall which would lead to rupture. For this type of temperature distribution, creep only causes the high thermal compressive stresses on the inner surface to relieve rather quickly and cause the wall to carry load in its outer portions.

Because a large thermal gradient across the vessel wall does not appear to cause rupture, the more probable failure mode for rupture would occur at high uniform temperatures in the wall. When a significant portion, such as half of the vessel wall thickness or more, experiences temperatures at which ultimate strength of the head material is approximately 68.95 MPa (10 ksi) and this temperature level occurs over a fairly large area of the lower head, rupture would more likely occur. A more definitive estimate of the required distribution of high temperatures to cause rupture would require further analysis and additional high temperatures testing of the SA533 material.

The part of the lower head which could cause vessel wall rupture and which is more susceptible to creep than the SA533 material is the full penetration weld connecting the forging with the plate material in the head. This is because the welding process reduces ductility and, thus, allowable creep strains in the heat affected zone[6]. However, this weld is higher on the head and, based on this analysis and the postulated length of relocation time, it does not appear that high enough temperatures could be reached through a large enough portion of the wall to cause substantial creep strain in the weld.

Another area of concern for creep rupture is around the lower head penetrations. These penetrations consist of Inconel nozzles with sleeves fitted through holes approximately 2.54 cm (1 in.) in diameter bored in the lower head and welded at the nozzle base to the vessel inner surface. If rupture of the nozzle occurred, molten material could possibly flow down through the penetration until lower temperatures in the penetration walls froze the material in the tube. Again, because of the highly localized temperatures, the effect in penetrations would also seem to be localized but further investigation into the effect on the penetration assembly should be evaluated in more detail.

7.0 REFERENCES

1. Tolman, E. L. and Moore, R. A., "Estimated TMI-2 Vessel Thermal Response Based on the Lower Plenum Debris Configuration", Joint AIChE/ASME Heat Transfer Conference, High Melt Attach Phenomena Session, Houston, TX, July 24-27, 1988.

2. Smith, G. V., "Evaluations of the Elevated Temperature Tensile and Creep-Rupture Properties of C-M_o, M_n-M_o, and M_n-M_o-N_i Steels", Metal Properties Council, American Society for Testing and Materials, ASTM Data Series Publication DS47, 1971.

3. Reddy, G. B. and Ayers, D. J., "High Temperature Elastic-Plastic and Creep Properties for SA533 Grade B Class 1 and SA508 Materials", Electric Power Research Institute Report No. NP-2763, December 1982.

4. Lemon, E. C., "COUPLE/FLUID, a Two-dimensional Finite Element Thermal Conduction and Convection Code, EG&G Idaho Report,ISD-SCD-80-1, February 1980.

5. "ABAQUS User's Manual (Version 4.6)", Hibbitt,Karlsson & Sorensen, Inc., Providence, Rhode Island, 1987.

6. V. N. Shah ltr to C. R. Toole, VNS-028-85, Severe Accident Extension Project, December 12, 1985.

APPENDIX A

HIGH TEMPERATURE MATERIAL DATA FOR SA533

This appendix contains experimental data results from Reference 3 which were used in this analysis. Figure A-1 plots stress-strain curves from the tensile tests performed. Young's Modulus and proportional limit stress for various temperatures determined in these tensile tests are shown in Figure A-2.

Figures A-3 through A-6 compare creep strain test data with the constitutive creep law developed in Reference 3. This creep law was determined by curve fitting the test data to a power function having parameters which are a function of temperature and stress. Figure A-7 shows this creep law as extracted from the referenced report. Comparison of this creep law with the law as modeled in ABAQUS is discussed in Section 5.0 of this report.

Coefficients of thermal expansion reported in the reference are instantaneous values. Mean values from an ambient reference temperature were calculated from these instantaneous values and are listed in Table A-1. These mean values were used in the model.

Contents

Figures

Table

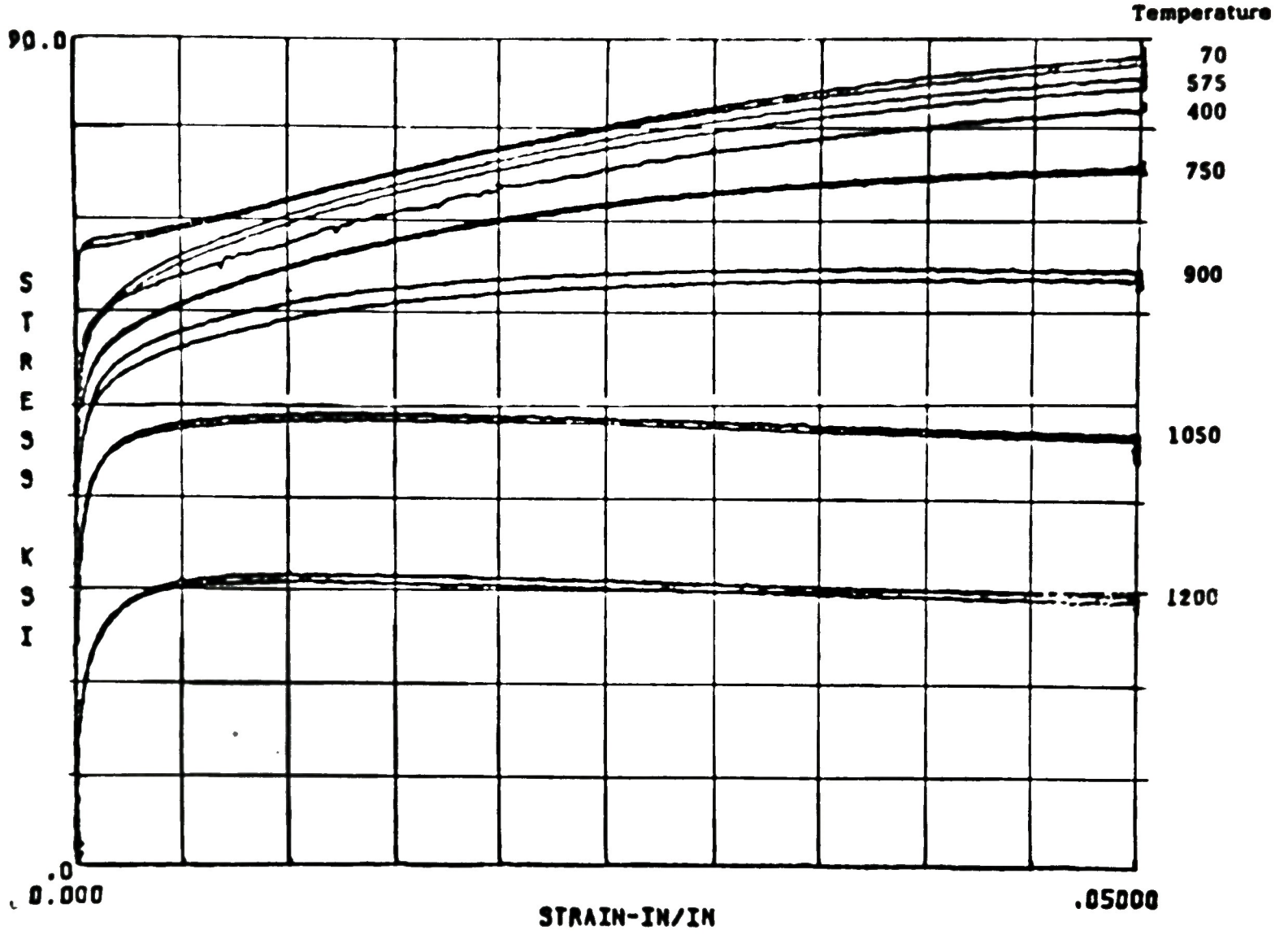

Figure A-1 - Stress-Strain Curves in the Range of 70 - 1200°F Temperature, 0 - 5 percent strain for SA533 Material

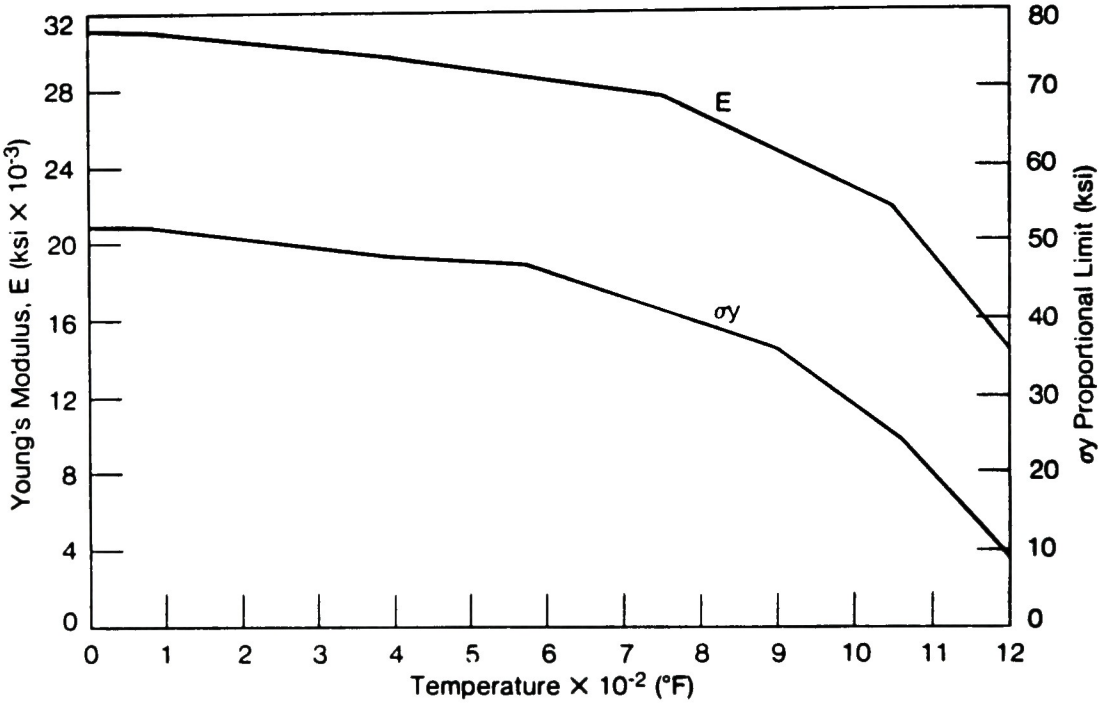

Figure A-2 - Young's Modulus and Proportional Limit Stresses for SA533 Material in the Temperature Range of 0 - 1200°F

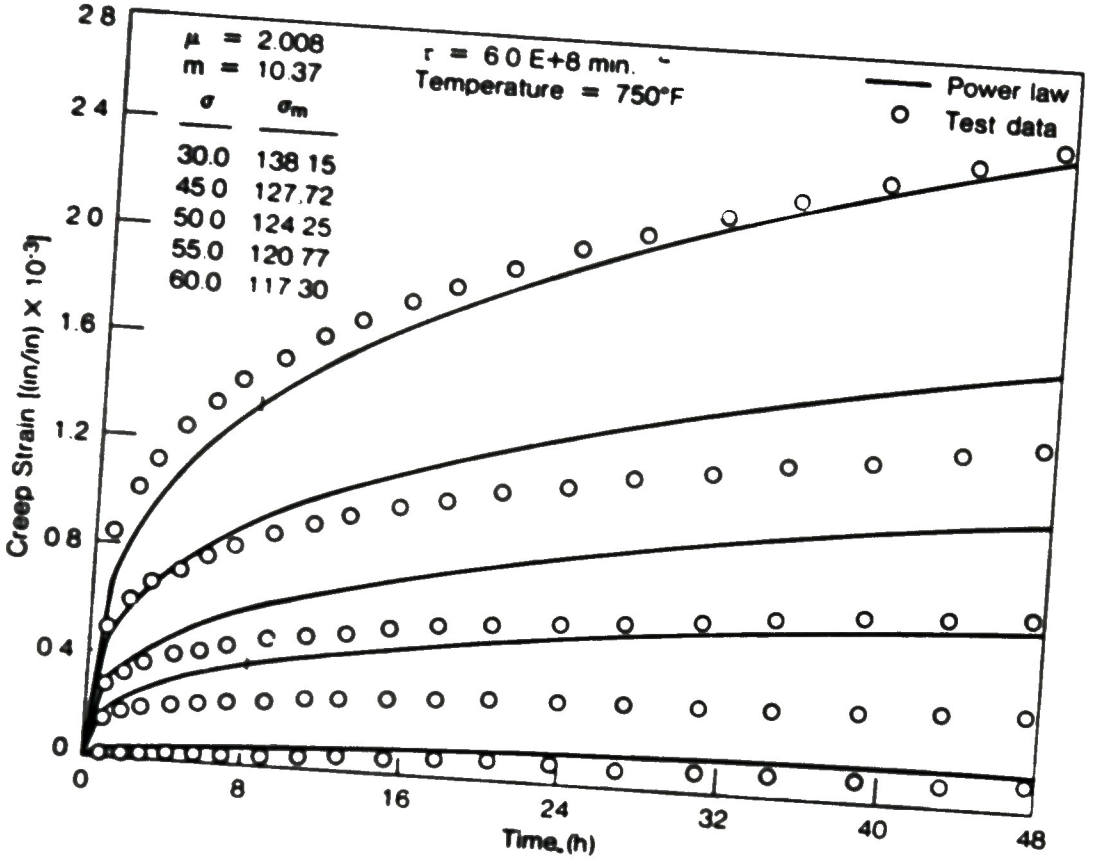

Figure A-3 - Comparison of Analytical Expressions and Test Data for SA533 Material Creep Properties at 750°F

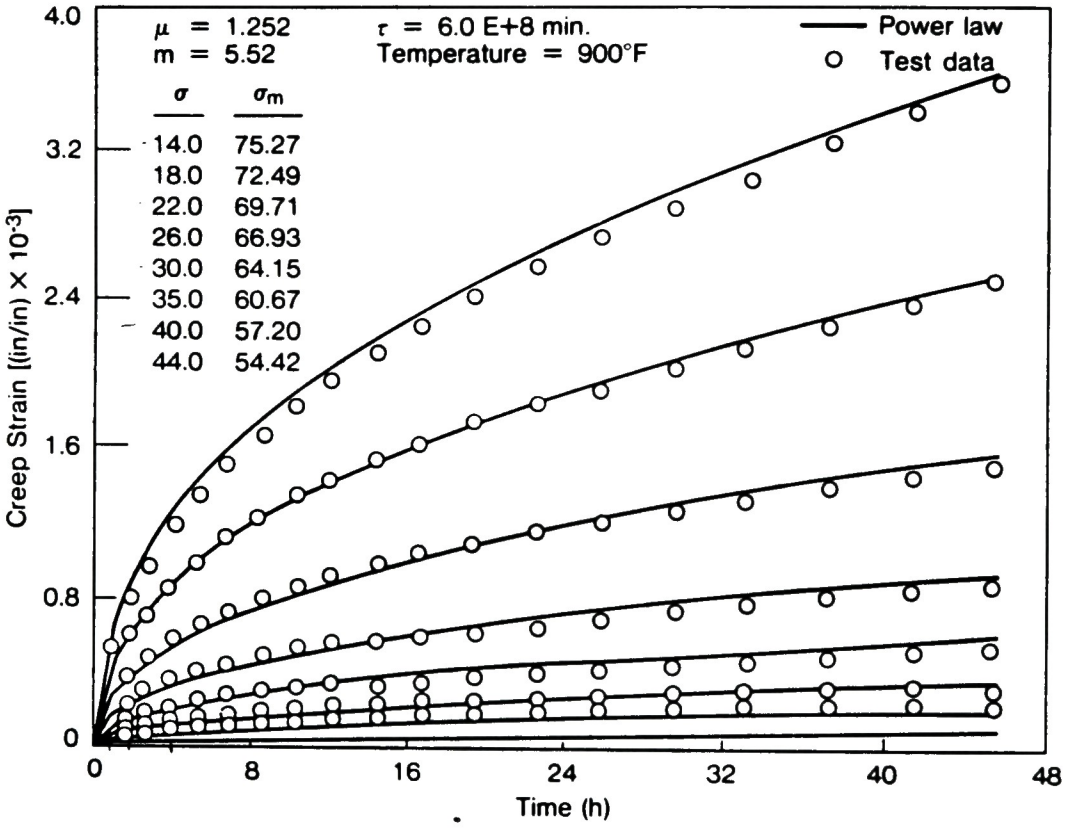

Figure A-4 - Comparison of Analytical Expressions and Test Data for SA533 Material Creep Properties at 900°F

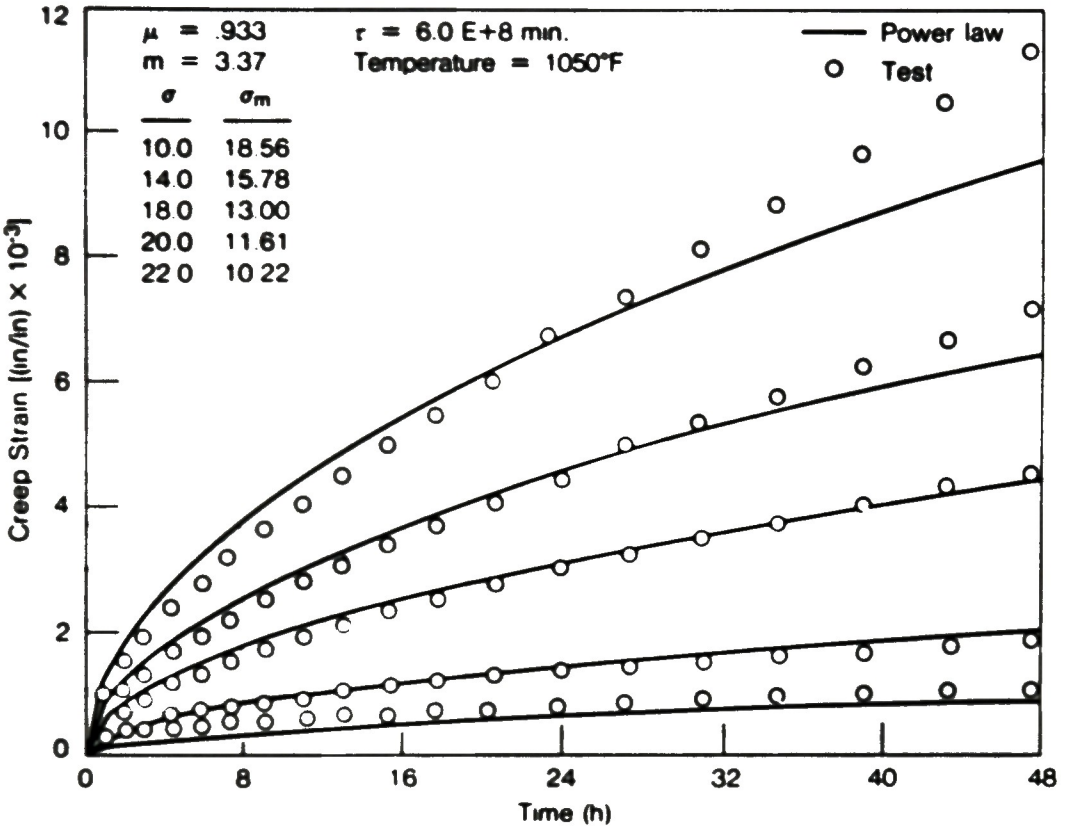

Figure A-5 - Comparison of Analytical Expressions and Test Data for SA533 Material Creep Properties at 1050°F

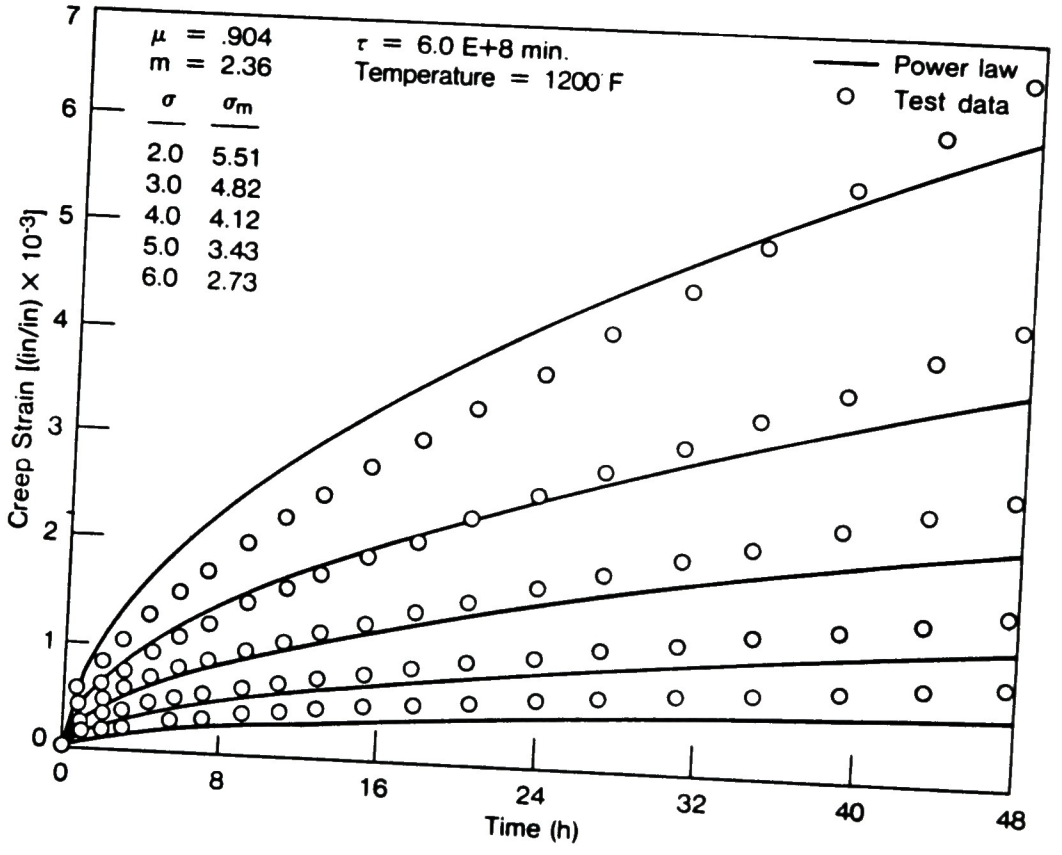

Figure A-6 - Comparison of Analytical Expressions and Test Data for SA533 Material Creep Properties at 1200°F

$$\varepsilon_c = \left(\frac{1+\mu}{\tau}\right)^{\frac{1}{1+\mu}} \left(\frac{\sigma}{\sigma_m}\right)^{\frac{m}{1+\mu}} (t)^{\frac{1}{1+\mu}}$$

where: ε_c = creep strain, in/in

τ = 6.0×10^8, min.

σ = stress, psi

t = time, min.

and:

$$\log_{10}\left(\frac{1}{1+\mu}\right) = -.1999429E+01 + .3020073E-02(T) - .1322426E-05(T)^2$$

$$\log_{10}\left(\frac{m}{1+\mu}\right) = .1276977E+01 - .9858134E-03(T)$$

$$\sigma_m = a - .695(\sigma)$$

$$\log_{10} a = .1507683E+02 - .3434874E+01(\log_{10} T)$$

for $700^\circ F \leq T \leq 900^\circ F$

$$\log_{10} a = -.1133500E+03 + .8682466E+02(\log_{10} T) - .1583739E+02(\log_{10} T)^2$$

for $900^\circ F \leq T \leq 1200^\circ F$

T = temperature in $^\circ F$

Figure A-7 - Creep Law from Reference 3

Table A-1

Mean Coefficients of Thermal Expansion
in the Range of 70-1200°F

Temperature (°F)	Mean Coefficient ($\times 10^{-6}$ in./in./°F)
547	7.13
600	7.20
800	7.63
1000	7.98
1200	8.35